WP3 Environmental impact & safety

Thermal changes and borehole stresses due to Eavor-Loop exploitation

Project name	ELFO: Eavor Loop Feasibility for Tilburg (Amer network) and Outlook for application in the Netherlands	
TKI reference	1921406	
Duration	01/11/2021 – 31/01/2023	
Work package	WP3 – Environmental impact & safety	
Dissemination level	Public	
Lead author(s)	Jan-Diederik van Wees (TNO)	
Contributors	Anna Rogers (Eavor), Peter Fokker (TNO), Al Moghadam (TNO)	
Verified (WP leader)	Jan-Diederik van Wees (TNO)	Date: 15/12/2022
Approved (coordinator)	Maartje Koning (TNO)	Date: 31/01/2023
Version	2.0 (revision 1; dated 30/08/2023)	

TKI URBAN ENERGY
Topsector Energie

The ELFO project has received funding through Topsector Energy (TKI Urban Energy programme) and these financial contributions are gratefully acknowledged. The contents of this publication reflect only the author's view and do not necessarily reflect the opinion of the funding agencies.

Het project is uitgevoerd met PPS-programmatoeslag subsidie van het Ministerie van Economische Zaken en Klimaat voor TKI Urban Energy, Topsector Energie. www.tki-urbanenergy.nl.

Executive summary

The Eavor-Loop (EL) is a closed loop geothermal energy production system based on a closed loop concept in which heat is extracted from the deep subsurface by heat conduction. The main objective of ELFO is to assess the applicability of the Eavor loop technology as the primary heat source for city heating networks in the Netherlands. This is accomplished through a feasibility study for the heat network in Tilburg and by providing an outlook for wider adaptation in the Netherlands.

This report covers WP3 Assess environmental impact, safety and CO_2 footprint of Eavor-Loop based on numerical simulations over its lifetime, capable of ruling out unsolicited effects (i.e., leakage, well bore collapse, induced seismicity), and validating low carbon footprint compared to conventional geothermal applications. The methodological approach includes the following steps

- Input well path trajectory, well completion and Eavor-Loop operational conditions (i.e., flow rate, inlet temperature) for the Tilburg Case study as well as relevant subsurface data and interpretation, thermo-mechanical properties have been adopted from the results of WP1 and WP2 of ELFO.
- Eavor-Loop performance and near well bore thermal response, based on thermal simulation
- Stress response as a function of the predicted near well bore thermal response, superposed on the in-situ stress.
- Analysis of Borehole stability and potential for fault reactivation.
- Subsequently, based on the thermal performance and Eavor-Loop construction and operational characteristics, LCA analysis (Life Cycle Assessment) and quantitative assessment of the CO_2 per GJ produced has been done.

In the Tilburg area the considered Eavor-Loop follows the Eavor-Loop 1.0 sedimentary design targeting the Triassic sandstones at ca 3200 m depth with 12 laterals. The layout of the wells is based on key well survey points which have been defined by Eavor. For the operation of the Eavor Loop it is assumed that inlet temperatures will be ~60°C and flow rate of 60 kg/s with the assumption that the water density at 60°C is 1000 kg/s. A dedicated numerical thermal model has been used to calculate the thermal response of the Eavor Loop for a lifetime of 10 years and 30 years at constant flow rate conditions. The grid sizes in radial direction have been chosen such that the logarithmic value of the cell centers radial coordinates is linearly increasing from sub cm-size at the well bore to few meters size a radial distance of 70 m, which is sufficient to fully cover the transient heat flow over the simulated lifetime. The predicted thermal power is in excess of 7 MWth.

The simulations indicate that the Eavor-Loop has a long lifetime marked by a very moderate linear decline of the production temperature and power over a lifetime of 10s of years, with minor thermal interference of laterals if placed with a spacing of ca 70 m (Holmes et al., 2021, Van Wees, 2021)

Based on the thermal simulations, we analyzed stress changes with a semi-analytical approach and conclude the following on borehole-stability (and potential leakage), potential for reactivation of pre-existing faults and underlying sensitivities.

Borehole stability:

- The borehole wall upon cooling of the Eavor-Loop is stable, except for less than 1 cm of the wall at the entry of the laterals, marked by a Shear Capacity Utilization (SCU) close to or slightly exceeding 1 indicative for frictional instability (in horizontal direction) and strong tensile stresses of -14 MPa (in vertical direction). According to the Cohesion of the reservoir rock as determined by lab experiments (Table 1) the SCU, which takes into account the regional stress field

characteristics and Cohesion, would remain below 1, except the first few mm at the borehole wall in horizontal direction, indicating shear stability of the borehole. However, the ca 14 MPa tensile stress will most likely lead to fractures due to tensile failure.

- The likelihood for tensile failure is dependent on the actual tensile strength which was not measured in the lab experiments as described in the WP1 results but can be estimated from Cohesion values. For the Triassic drilled in Tilburg, cohesion may not be higher than 3-6 MPa. Therefore, it will create tensile fractures under the ca 14Mpa tensile stress. However, these will be limited to the first few mm up to ca 1 cm of the borehole wall. In the analysis we did not consider the impact of Eavor's proprietary Rock-Pipe, which will be placed on the walls of the open hole laterals to seal off the formation from the fluids inside the EL. This could change the rock parameters at the wellbore face, and can to some extent affect the cohesion, friction, and tensile strength.
- The thermal effects, responsible for the tensile fracturing will manifest themselves very early in the Eavor Loop lifetime, possibly already during drilling when mud circulation is causing borehole wall cooling. The fracturing can therefore already occur during the drilling process. Stress effects of thermal cooling do not noticeably increase over time after the first month of operation. Consequently, the breaching of Rock-Pipe, after the first month of operation is unlikely, and prevention of leakage can be enhanced by deliberately generating thermal stress effects during drilling promoting potential fractures. The early use of Lost Circulations Material (LCM) and Rock-Pipe to plug the crack tip can prevent further propagation. Rock-Pipe can be reapplied throughout the life of the Eavor-Loop. In addition, Eavor can carefully design drilling and operating pressures and circulating fluid densities so as to not exceed the fracture gradient throughout the life of the Eavor-Loop.

Potential reactivation of faults:

- Stress effects have been calculated up to 70 meters from the well bore based on the predicted temperature response at 120 months and have been tested for stability on pre-existing fracture favorably aligned in the (locally rotated) stress field, adopted a cohesion of 0.
- The results show Shear Capacity Utilization (SCU) for pre-existing fractures leading to failure only in the very close vicinity of the borehole (<10 m radius). The associated reactivated fault areas would be relatively small and most likely not result in seismicity which could be felt at surface – unless stress changes are able to trigger theoretically larger events, albeit at much lower probability.

Sensitivities:

- The results for potential fault reactivation are very sensitive to the in-situ stress assumptions. Adopting a higher horizontal stress gradient of 17 MPa/km instead of the base case 15 MPa/km, results in more stable predictions, both in terms of SCU for fault reactivation, as well as tensile stresses at the bore hole wall, positively affecting borehole stability.
- The sensitivity to fault reactivation has been analyzed for a higher estimate of the friction angle of pre-existing faults (in line with the range given in Table 1). This results in reduced SCU values, preventing shear failure for existing faults. Well bore stability is still prone to high tensile stresses.
- Lower injection temperature will result in larger cooling of the well bore, in particular at the bore hole wall. In order to test the sensitivity to lower injection temperature the injection temperature was reduced from 60°C to 40°C. Consequently, the amplitude of the stress changes is enlarged and results in more accentuated bore-hole instabilities and a potentially larger instable zone for frictional reactivation of pre-existing faults, further away from the borehole.

Subsequently, based on the thermal performance and Eavor-Loop construction and operational characteristics, LCA analysis and quantitative assessment of the CO_2 per GJ produced has been done in comparison to a conventional geothermal doublet system:

- The emission characteristics (kg CO_2-eq/GJ) of the Eavor-Loop are ca 20% improved compared to a conventional geothermal doublet system, saving over 2 kg CO_2-eq/GJ. In more detail, emission related to construction is slightly higher than a conventional doublet, related to much longer drilled sections. However, the operation related emissions marked by reduced pumping power and absence of formation gas compared to a conventional doublet system, and offset the increase related to construction.

Contents

Tables

Figures

1 Introduction

1.1 ELFO project

The Eavor Loop (EL) is a closed loop geothermal energy production system based on a closed loop concept in which heat is extracted from the deep subsurface by heat conduction. The main objective of ELFO is to assess the applicability of the Eavor loop technology as the primary heat source for city heating networks in the Netherlands. This is accomplished through a feasibility study for the heat network in Tilburg and by providing an outlook for wider adaptation in the Netherlands. The following subobjectives are included:

WP1 Assess subsurface suitability in the Tilburg Area for construction of an EL, and prognose associated heat delivery as function of subsurface and (design) engineering parameters.

WP2 Design a dedicated EL rig development for cost effective drilling and completion of the proposed EL, such that the drilling can be carried out cost effectively on a 24/7 basis in the urban environment.

WP3 Assess environmental impact, safety and CO_2 footprint of EL based on numerical simulations over its lifetime, capable of ruling out unsolicited effects (i.e., leakage, well bore collapse, induced seismicity), and validating low carbon footprint compared to conventional geothermal applications.

WP4 Develop an optimized EL design and operational parameters for integration in Amer heat network, addressing required heat demand profiles, temperature levels, and business case.

WP5 Provide an outlook for EL in the Netherlands, including best practices and a roadmap for use in similar and different geological settings.

1.2 WP3 goals and objectives

The following aspects of environmental impact & safety are being addressed in this report:

- Induced seismicity, well integrity (and leakage) risks have been assessed with thermo-mechanical models, simulating thermal strains and stress changes close to and further away from the wells, at a representative section of the lateral, most prone to risks (cooling). Temperature changes are used as input for the calculation of stress changes using (semi-) analytical models as much as possible, complemented and benchmarked with numerical codes where needed.
- The resulting stresses are strongly dependent on both the thermal expansion coefficient, and elastic properties, and stratification thereof (input from WP1). WP3 performed a comprehensive sensitivity study on the range of stress changes as a function of rock properties, geometry of the well as the effects of temporal changes over the operational lifetime.
- The inferred stress changes have been interpreted in terms of their potential contribution to destabilization of the bore hole wall and potential well leakage, and potential seismic slip-on natural faults and fractures crossed by the laterals. The stress changes, potential for seismic slip, well bore stability, potential leakage have been interpreted over the lifetime of the Eavor-Loop as a function of progressive cooling of the borehole wall.
- CO_2 footprint: The CO_2 footprint of the Eavor-Loop has been analyzed in view of alternative geothermal systems. This concerns an LCA analysis for construction of the EL, as well as

assessment of greenhouse gas emissions of the EL, related to circulating the working fluid. This activity will result in a quantitative assessment of the CO_2 per GJ produced EL.

1.3 Approach

The energy output over time of an Eavor-Loop™ system can be predicted using various engineering approaches to model the transient heat transfer from the surrounding rock to the fluid flowing through the wellbore. Two methods can be used; the first is a numerical solution of the transient, two-dimensional (2-D) heat conduction equation for the rock coupled with the one-dimensional energy equation for the fluid flow in the wellbore. The second and more rigorous approach is a full transient, three-dimensional (3-D) numerical simulation of the heat transfer in the rock and heat transfer and turbulent flow of the fluid flow in the wellbore.

The approach for the study on environmental impact & safety, includes

- Input well path trajectory, well completion and Eavor-Loop operational conditions (i.e., flow rate, inlet temperature) for the Tilburg Case study as well as relevant subsurface data and interpretation, thermo-mechanical properties have been adopted from the results of WP1 and WP2 of ELFO.
- Eavor-Loop performance and near well bore thermal response, based on thermal simulation
- Stress response as a function of the predicted near well bore thermal response, superposed on the in-situ stress
- Analysis of Borehole stability and potential for fault reactivation.

The steps are outlined in Figure 1. Further details for the numerical models for the thermal and stress response are given Appendix A and Appendix B, respectively. The Input well path trajectory, well completion and Eavor-Loop operational conditions (i.e., flow rate, inlet temperature)

Subsequently, based on the thermal performance and Eavor-Loop construction and operational characteristics, LCA analysis and quantitative assessment of the CO2 per GJ produced has been done.

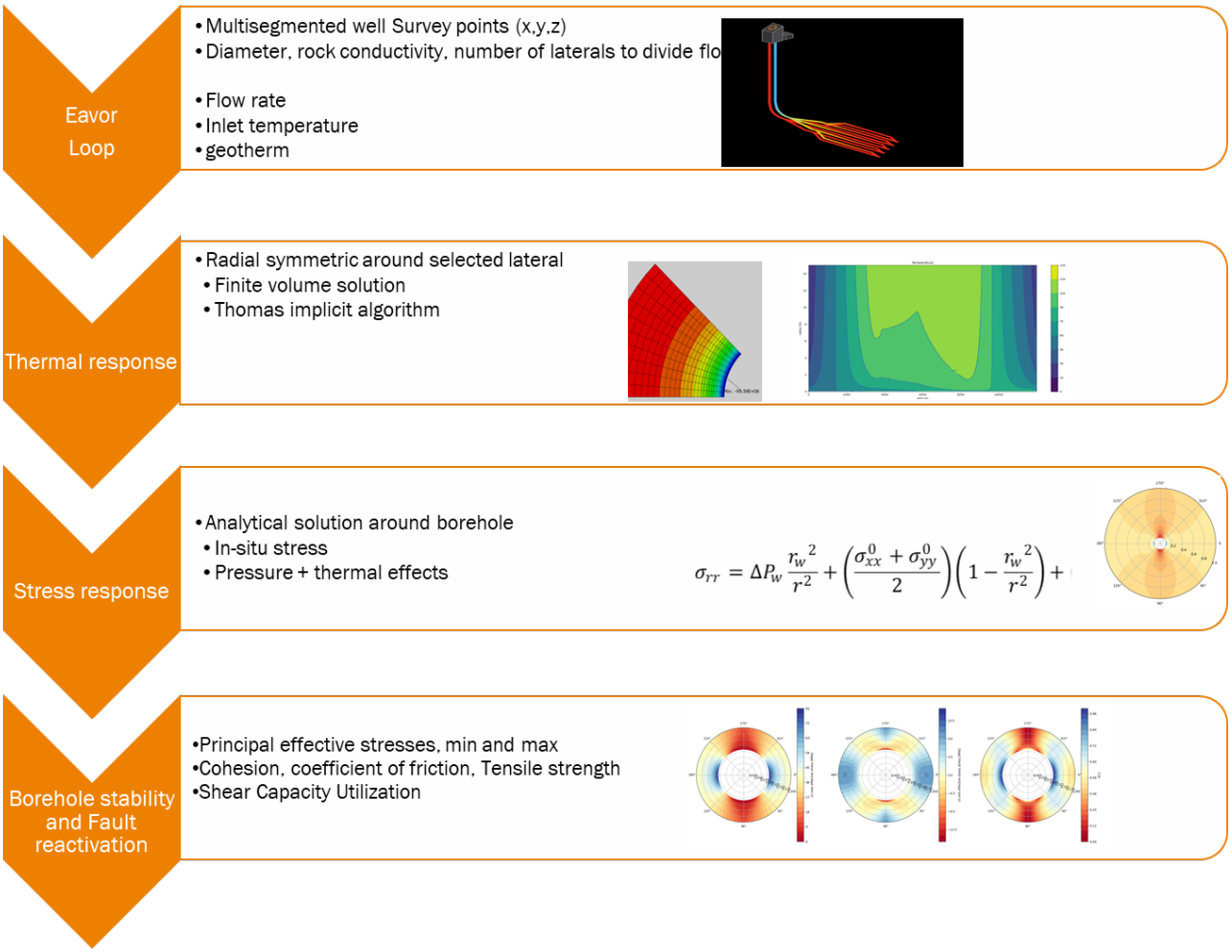

Figure 1 Schematic approach for determinization of thermal performance of the Eavor-Loop and analysis of borehole stability and potential for fault reactivation.

2 Input data Tilburg Eavor-Loop

In the Tilburg area the considered Eavor-Loop is a so-called James Joyce chain design (Figure 2) with 12 laterals. The layout of the wells is based on key well survey points which have been defined by Eavor (Figure 3).

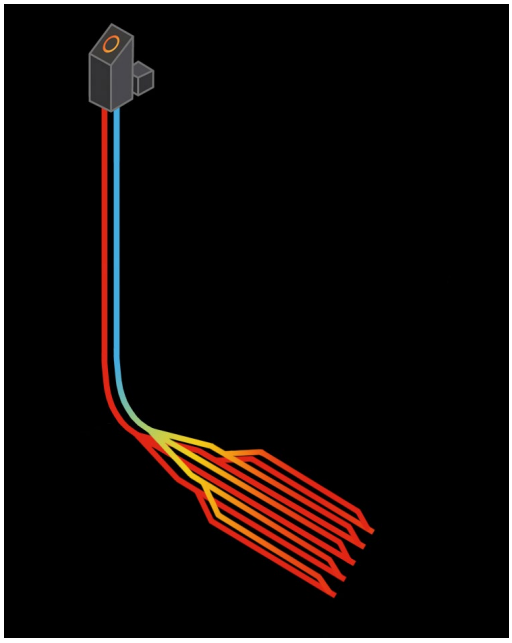

Figure 2 Schematic diagram of a James Joyce Design for the Eavor-Loop considered in Tilburg area.

Eavor™

Horizontal Geological Prognosis (WIF)

Location:					
	Well Name:	Tilburg-EL-v0	Date Initiated:	2022-07-01	
	Area / Field Name:	Tilburg, Netherlands	Date Page 1 Revised_Version:		v0
	Well Classification:	1.0	Reference Datum (GL):	9.00	
	Hz Target Zone:	Trias. Buntsandstien	Rig KB	TBD	
	AFE Number:		Rig #:	TBD	
	Lease/Pad:	Attero	Cellar:	TBD	
	Upper/Lower Well	Lower	Avg. Hz Length	2000.0	

Amersfoort RD New (EPSG28992):	Easting / X:	Northing / Y:	SS Elevation :
Surface Location:	132505.2	401253.5	9.0
Kick-Off Point (KOP):	132505.2	401253.5	-3025.0
Intermediate Casing Point (ICP):	132777.0	400843.1	-3425.0
Number of legs	12		
Multilateral Leg Inclination	95°		
Multilateral Leg Azimuth	169°		
Vertical Leg Spacing	65m		
Horizontal Leg Spacing	65m		
Bottom hole TD Target	133275.5	398727.1	-3125.0

Figure 3 Well survey points for the James Joyce Design in Tilburg. The ICP is interpreted as the point where the laterals (and subbranches) are interpreted to start. The endpoint of the main lateral is at the Bottom Hole TD. It is assumed that given well survey points are the average depth of the laterals (so one is 10s of meters above, other 10s of meters below)

The survey points have been used to design a realistically drillable well path for the Eavor-Loop and lateral trajectories (Figure 4). The target horizontal and vertical spacing of the laterals and Build Up Rate (BUR) have been listed in Table 1.

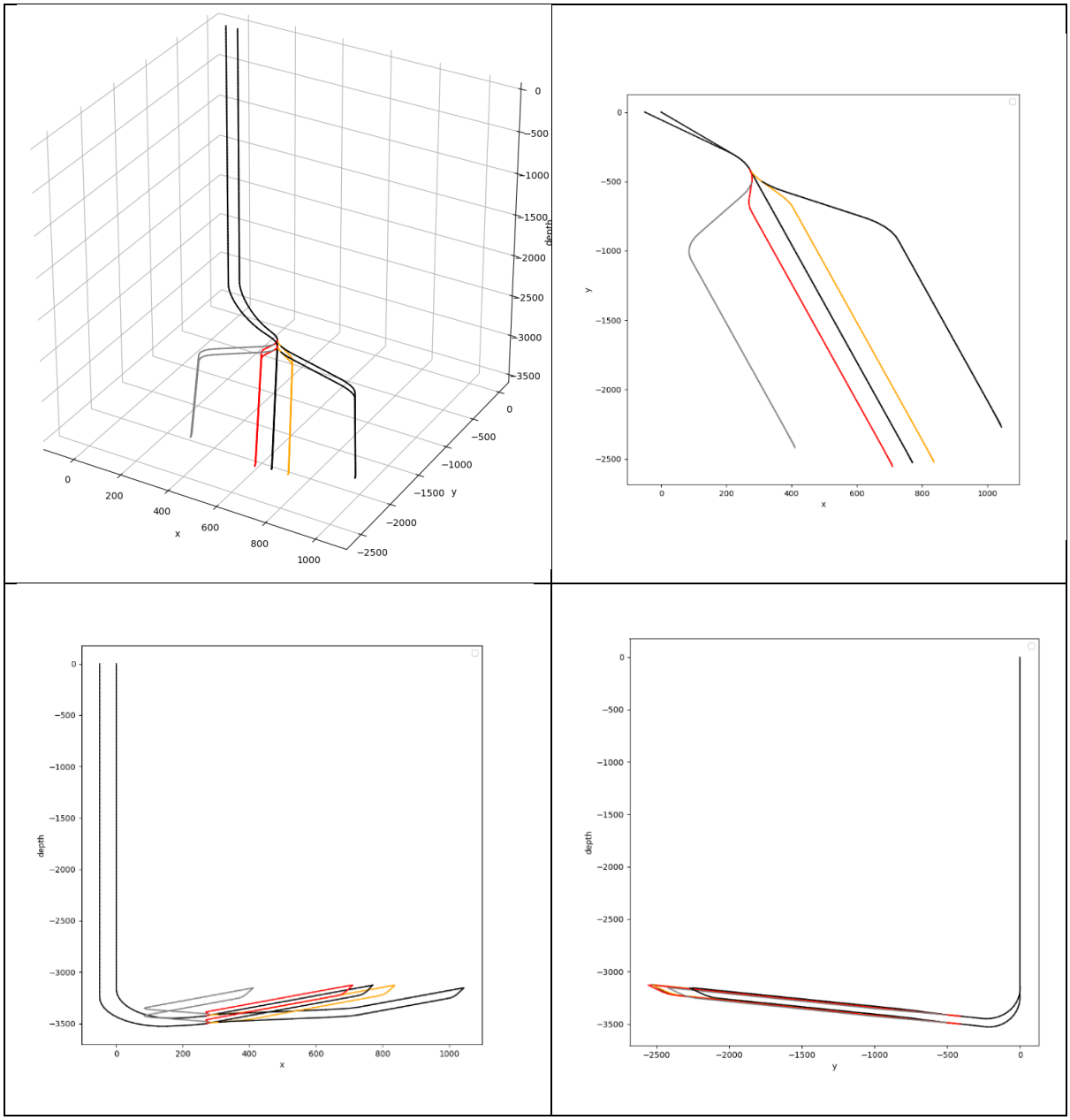

Figure 4 Main, 2 outer and 2 inner laterals (out of 12) illustrating the James Joyce design for the Tilburg area.

Table 1 Parameters used in the Tilburg Case study

parameter	value	unit	remarks
target formation	Triassic		
laterals			
lateral length (times two)	2180	m	see well survey points (Figure 4)
start depth	3450	m	see well survey points (Figure 4)
end depth	3125	m	see well survey points (Figure 4)
lateral dip	-7.8	degrees	see well survey points (Figure 4)
number of laterals	12		
horizontal spacing laterals	65	m	maximum lateral extent is 325 m from the main lateral
vertical spacing laterals	75	m	return is deepest located 32.5 m below specified depths, inlet is located 32.5 m above specified depths
Build Up Rate (deg/30m)	6		
diameter wells	8.5	inch	
thermal properties/model			
typical porosity	7	%	Tilburg area Triassic core plug porosities are in the range 6-10%, ~7% on average. 'Good' reservoir zones have 8-13% (5-26 mD), 'poor' zones 7-8% (0.06 – 0.5 mD) (BP report 'Sedimentology and reservoir quality of the Middle and Upper Bunter Formations')
conductivity laterals	3	W m-1 K-1	Limberger et al., 2019. The P3 petrophysical properties database (Bär Reinsch & Bott 2020) has average bulk thermal conductivities for Triassic sandstone (measured in Germany so likely comparable with the Netherlands) between 2.8 (fine sandstone) and 3.6 (coarse sandstone). 'Average' sandstone has 3.0. The latter is in line with Limberger. Chris Dalby core data measurements on Triassic sandstones (relatively nearby wells Werkendam, Waalwijk Noord, Steelhoven) has average 4.2 for horizontal, saturated.
conductivity vertical sections	2.25	W m-1 K-2	
rock heat capacity	3	MJ K-1 m-3	Limberger et al., 2017
fluid heat capacity	4.18	kJ K-1 kg-1	water
temperature model	Gies et al., 2021		See Figure 6
mechanical parameters			
Young's modulus	20	GPa	lab experiments (range 21 -25 GPa)
Poisson's ratio	0.2		lab experiments (range 0.05-0.16)
linear expansion coefficient	1.50E-05	K-1	lab experiments (range 0.9-2E-5)
cohesion	20	MPa	lab experiments (range 26-41 MPa)
friction angle	31	degrees	lab experiments (range 29-40 Degree)
in-situ stress			
SH (maximum total horizontal stress)	21	MPa km-1	oriented in direction of the lateral azimuth (~150°), stress report wUP
sh (minimum total horizontal stress)	15	MPa km-1	stress report wUP, perpendicular to lateral
sv (vertical total stress)	22	MPa km-1	stress report wUP
hydrostatic pressure	10.6	MPa km-1	brine

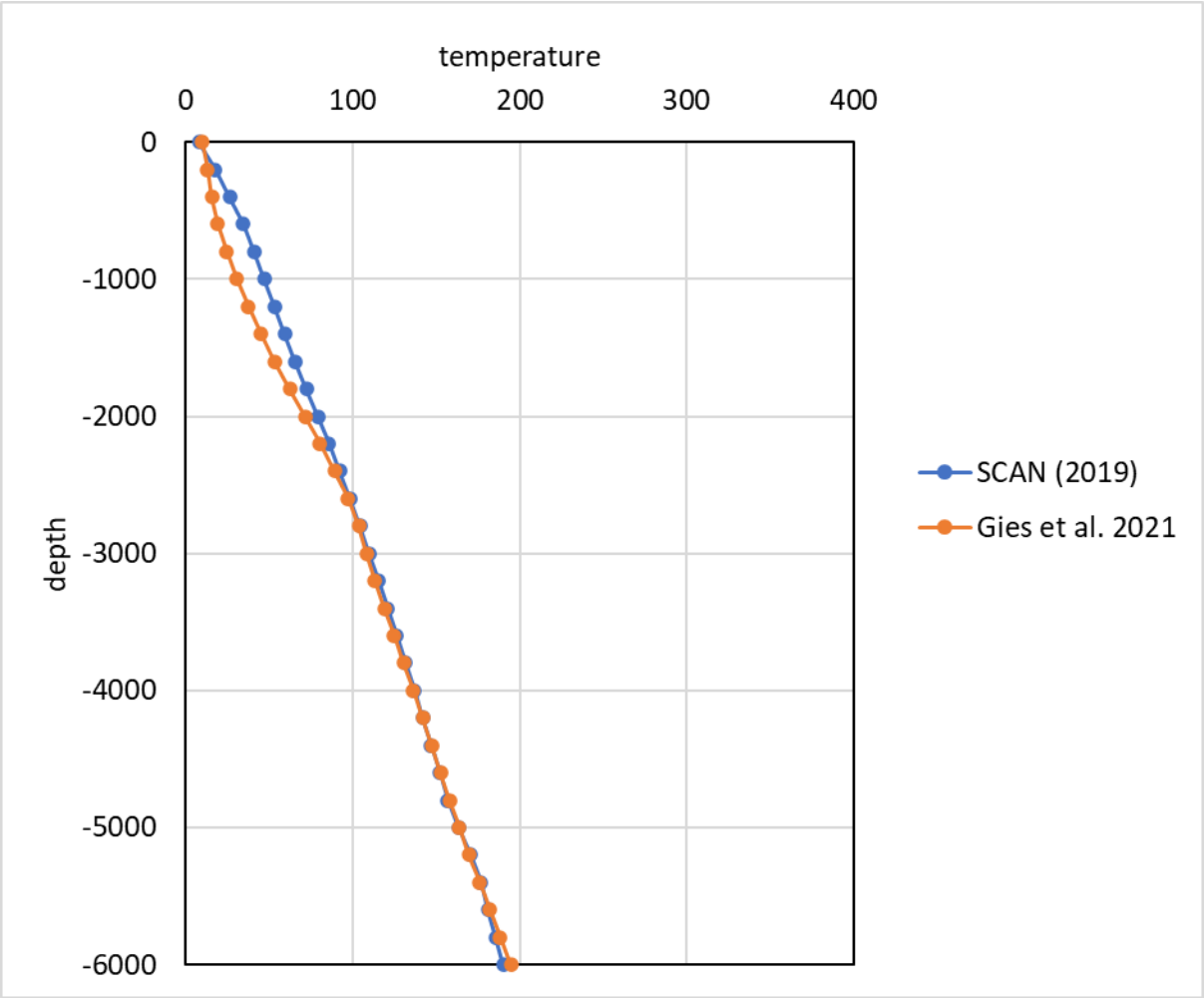

Figure 5 Temperature model for the Tilburg area, according to SCAN (2019) and Gies et al. (2021)

3 Thermal analysis Tilburg Eavor-Loop

The heat transfer for the Eavor Loop system occurs through thermal conduction, proportional to the thermal gradient at the Eavor Loop bore hole wall. The thermal gradient is largest at the initial stage of operation and gradually declines due to progressive thermal diffusion (this phenomenon is illustrated in Figure 10).

For the operation of the Eavor Loop it is assumed that inlet temperatures will be ~60°C and flow rate of 60 kg/s with the assumption that the water density at 60°C is 1000 kg/s.

The thermal model introduced in section Appendix A has been used to calculate the thermal response of the Eavor Loop for 10 years at constant flow rate conditions. The discretization of the simulation grid is depicted in Table 2. The grid sizes in radial direction have been chosen such that the logarithmic value of the cell centers radial coordinates is linearly increasing. This results in order cm-size cell radial size of first grid-cells surrounding the wells.

The extent of the grid in radial direction is sufficient to fully cover the transient heat flow over the simulated lifetime, as shown later.

The results for the thermal response are shown in Figure 6 and Figure 7.

Table 2 Simulation grid specification for the Tilburg Eavor Loop

parameter	Value	unit
total length	11992	m
number of segments (along hole)	100	
extent of grid in radial direction	70	m
number of grid cells in radial direction	50	
start laterals	3450	m
end laterals	8170	m
number of laterals	12	

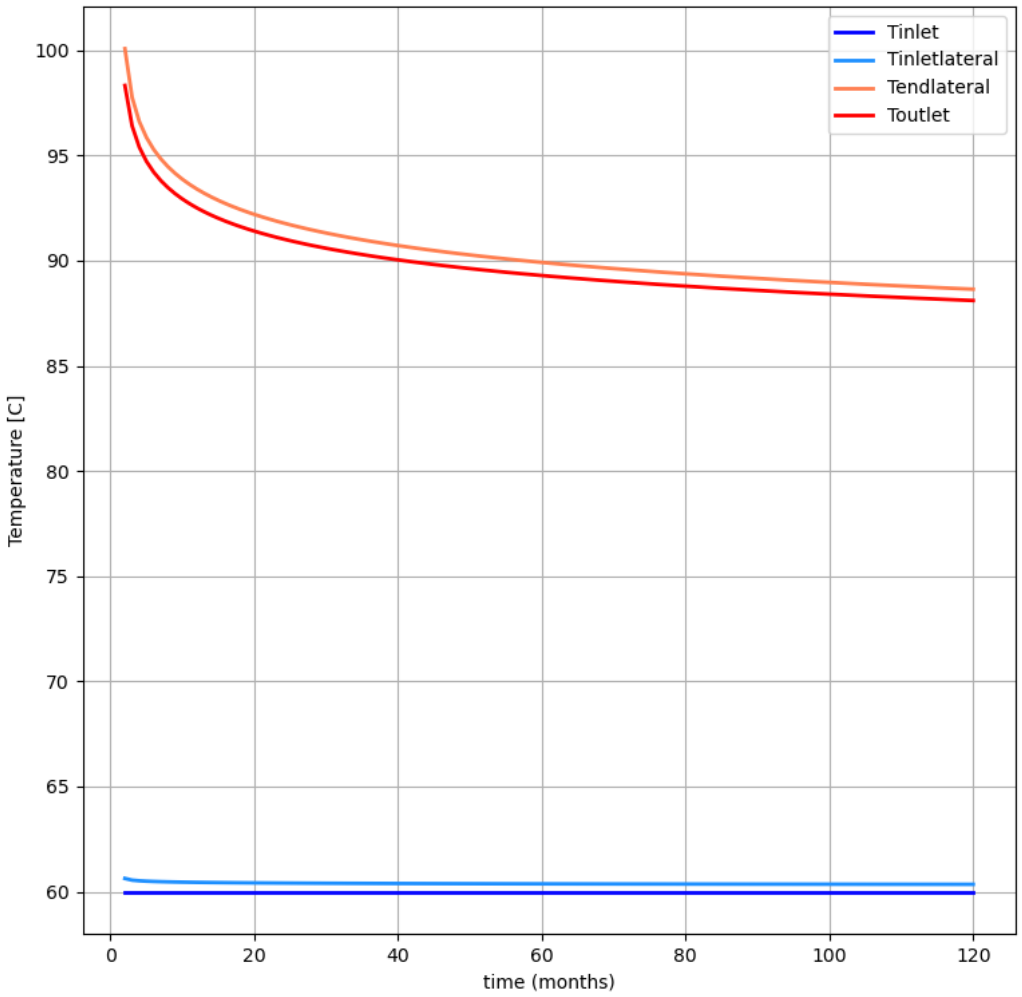

Figure 6 Thermal response of the Tilburg Eavor Loop. The Tinlet, Toutlet correspond to EL fluid temperatures at the start (AHD=0) and end (AHD=11992m) of the EL trajectory in Figure 7. TinletLateral, Tendlateral correspond to the EL fluid temperatures at the start and end of the lateral section of the multi-lateral section, denoted in blue in Figure 7.

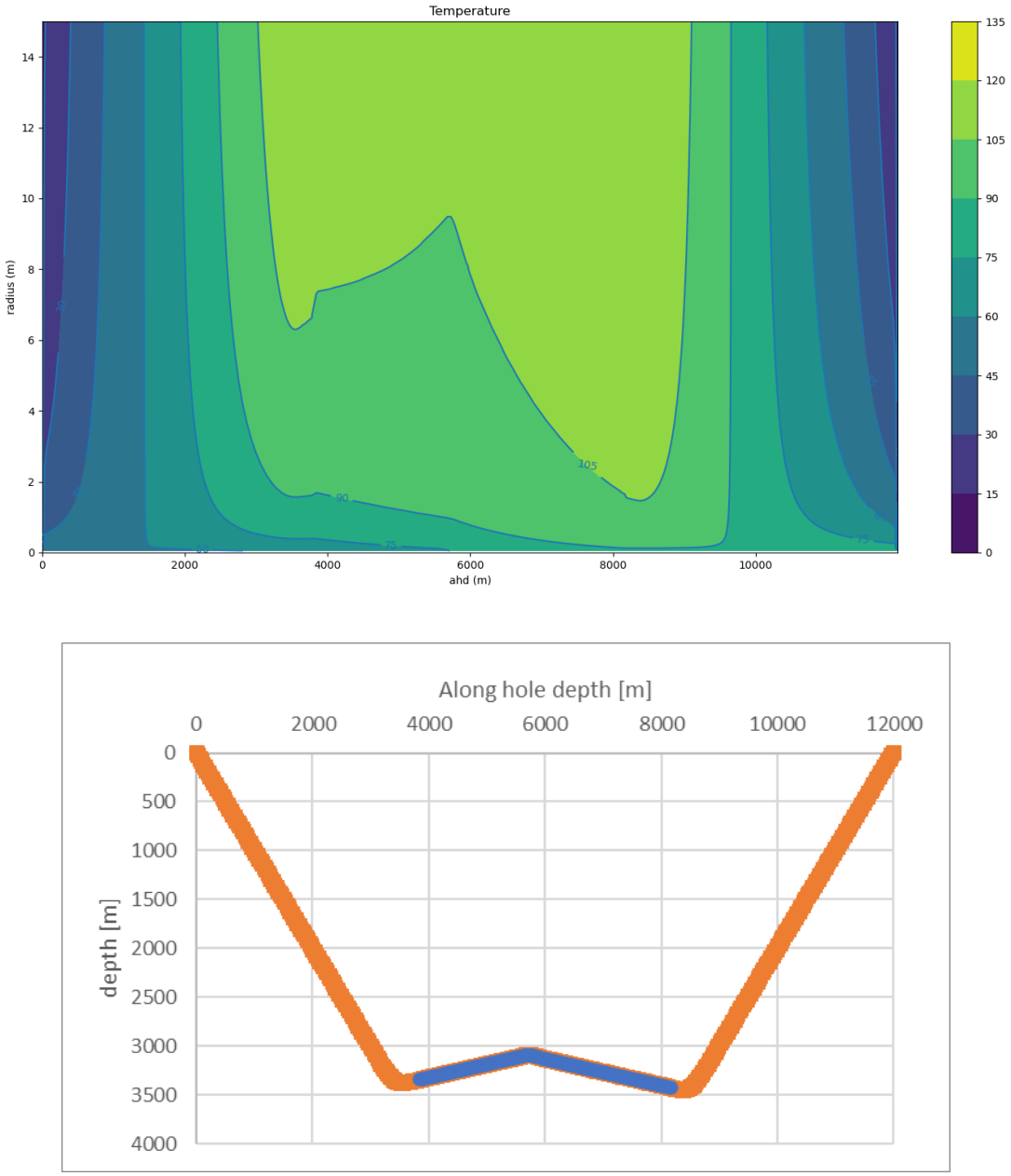

Figure 7 (top) Temperature around the main lateral (radius, on vertical axis) as a function of along borehole Depth (AHD, on horizonal axis) along the loop at 120 months of operation, (bottom) True vertical depth as a function of along hole depth. The blue section marks the multi-lateral lateral section (cf Figure 4).

The predicted thermal power is in excess of 7 MWth.

3.1 Long term outlook

In order to illustrate the different effects of long-term operational usage on the thermal power and thereby the capacity of the system, the model simulations were extended for a longer lifetime of 30

years. The results and differences compared to shorter operational time spans are illustrated in the figures below.

Figure 8 shows the temperature change along the axis of the Eavor Loop (central lateral) and the rock cooling surrounding the Eavor Loop are shown in Figure 9 and Figure 10, respectively.

These figures can be compared with Figure *6* and Figure 7. The production temperature is marked by a decline from ca 88.5C at 10 years of operation to ca 85.5C at 30 years of operation. This decline results in less than 10% reduction in power. The heat exchange effects in the earth layers surrounding the Eavor Loop after 30 years of operation are shown in Figure 9 and Figure 10. The heat exchange in the shallow subsurface are comparable to conventional geothermal doublet systems in the Netherlands, limited to a maximum of 20C heating in the close proximity of the borehole up to a radius of 10 m. At larger depth and in the lateral segments, rocks are significantly cooled, up to 40C in the very close proximity (< 1 m) of the Eavor Loop, whereas cooling up 20 C can occur to a radius of 10 m.

The thermal balance in the long term of the Eavor Loop system can best be described as a progressive cooling of sedimentary layers occurring in the vicinity of the vertical boreholes and laterals of the Eavor Loop. Whereas in the down flow and up flow vertical bore hole trajectory the rock layers are slightly heated (see Figure 9, middle). The rock temperature changes are occurring in the close vicinity of the Eavor Loop limited to a radius of ca 35 m of the Eavor Loop trajectory. The thermal changes in the rock will relax to original subsurface temperature conditions after termination of operation by thermal diffusion and natural heat flux of the earth.

Taking all simulation results into account, the Eavor Loop has a long lifetime marked by a very moderate linear decline of the production temperature and power over a lifetime of 10s of years, with minor thermal interference of laterals if placed with a spacing of ca 70 m (Holmes et al., 2021, Van Wees, 2021).

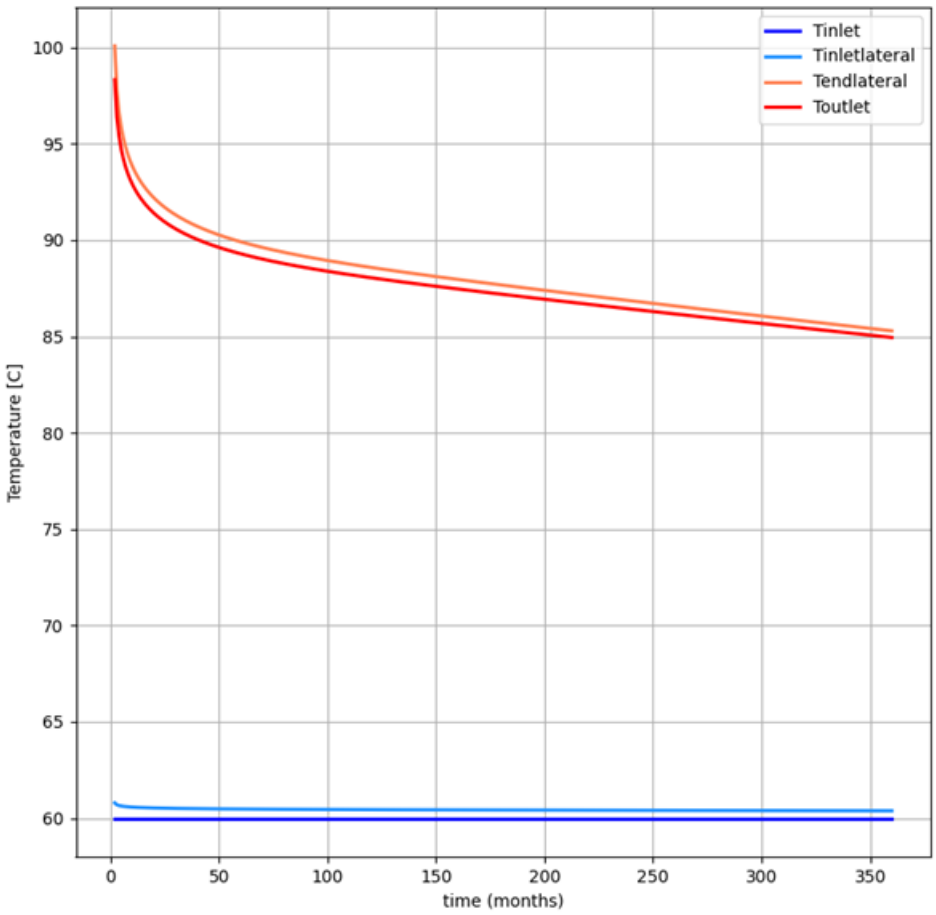

Figure 8 Thermal response of the Tilburg Eavor Loop (EL) for an extended lifetime of 30 years. The Tinlet, Toutlet correspond to EL fluid temperatures at the start (AHD=0) and end (AHD=11992m) of the EL trajectory in Figure 7. TinletLateral, Tendlateral correspond to the EL fluid temperatures at the start and end of the lateral section of the multi-lateral section, denoted in blue in Figure 7.

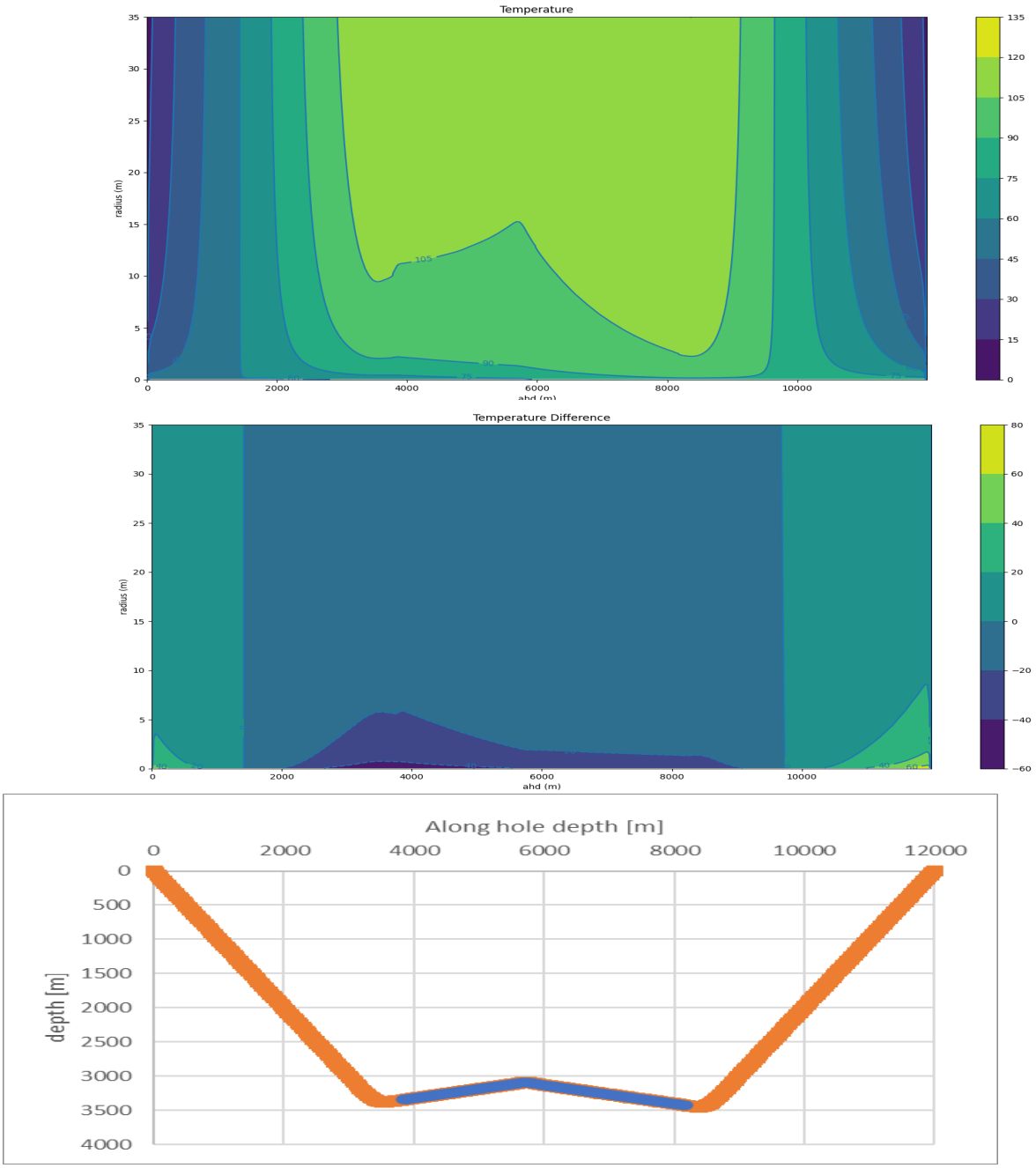

Figure 9 (top) Temperature around the main lateral (radius, on vertical axis) as a function of along borehole Depth (AHD, on horizonal axis) along EL at 30 years of operation, (middle) same but difference with original rock temperature, (bottom) True vertical depth as a function of along hole depth. The blue section marks the multi-lateral lateral section

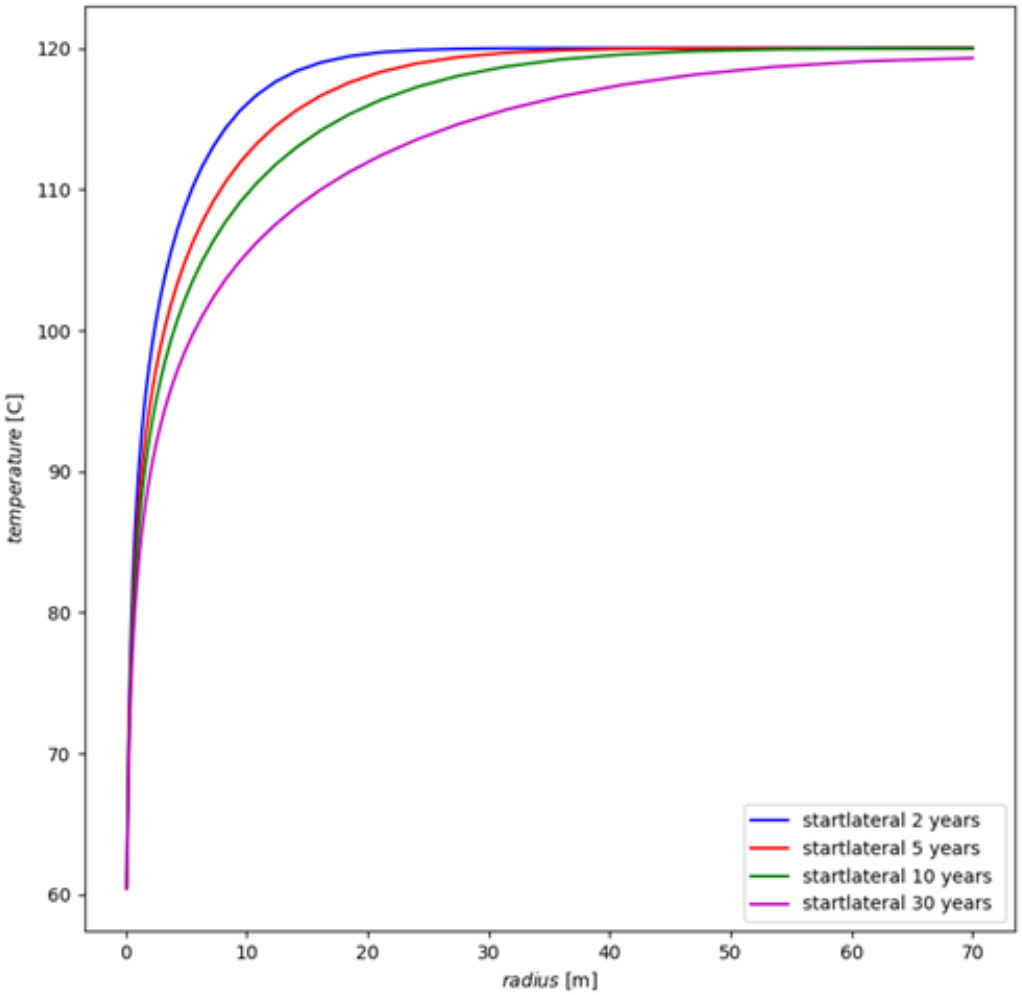

Figure 10 maximum cooling of rock layers surrounding the EL just before the onset of the lateral (at AHD 3600 m)

4 Stress effects due to Thermal Cooling of the Tilburg EL

The cooling relative to in-situ temperatures at depth is the largest at the entry of the injected water in the laterals which can be seen in Figure 7 at the start of the laterals at ca 3600 m AHD. At that position the predicted cooling around the borehole over time is given in Figure 11. In the analysis, positive stress values are compressive.

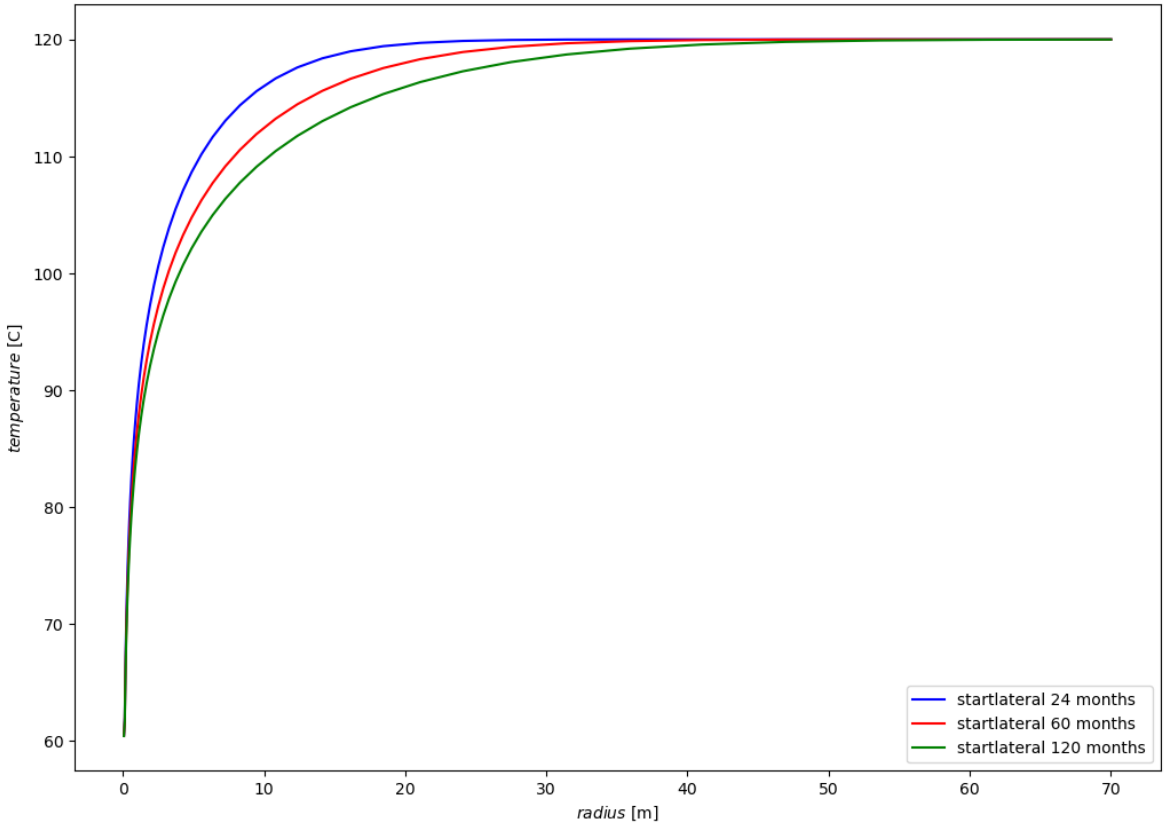

Figure 11 Predicted cooling at the 3600 m along hole depth at ca 3370 m TVD (just before the laterals start).

Figure 11 shows the resulting thermal stresses at 3600 m AHD (just before the laterals start) after 10 years of cooling, caused by the temperature differential from the well bore and in-situ rock temperature. This plot only shows the thermal stresses generated and does not include the interaction with the in-situ stresses component.

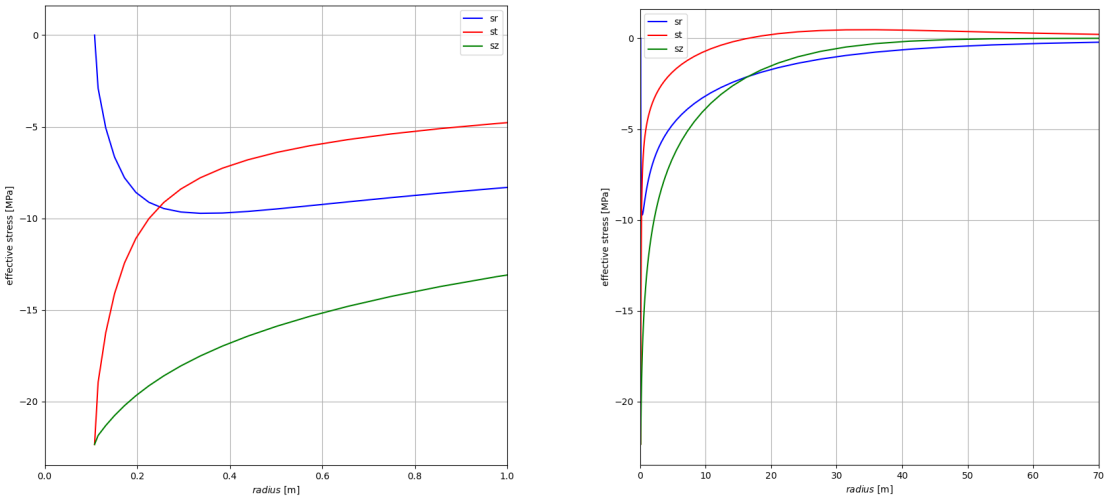

Figure 12 Thermal stress changes after 10 years of cooling (radial σ_{rr} (sr), tangential $\sigma_{\theta\theta}$ (st) and along hole stress σ_{zz} (sz). (left) up to 1 m radius, (right) up to 70 m radius

4.1 Well bore stability

Stress effects have been calculated near to the well bore based on the predicted temperature response depicted in Figure 11 at 120 months and have been tested for borehole stability. The stresses shown below include both the in-situ stress and thermal stress components. Parameters for the in-situ stress are given in Table 1. Well pressure has been assumed 2 MPa at the well head. Adopting fresh water in the well bore column and a relatively high hydrostatic pressure gradient to high salinity of brines (10.6 MPa/km), the difference in water pressure in the well and the formation is assumed negligible at a depth of 3400 m.

In the polar plots (Figure 13, Figure 14, and Figure 15), the view is looking down the lateral well bore, and the 0° corresponds to a horizontal orientation. The plots display the stress away from the well bore (radially) and around the well bore (circumferentially). The results show that very close to the borehole wall the stresses are marked by a high stress ratio and tensile stresses for the vertical direction.

The stress tensor can be used to calculate the coulomb stress change or Shear Capacity Utilization (Buijze et al., 2017). The SCU for a fault plane is defined as:

$$SCU = \frac{\sigma_s}{C + \mu\sigma'_n}$$

Where σ_s is shear stress, σ'_n is effective normal stress, C is cohesion and μ is the friction coefficient (corresponding to the tangent of the friction angle φ).

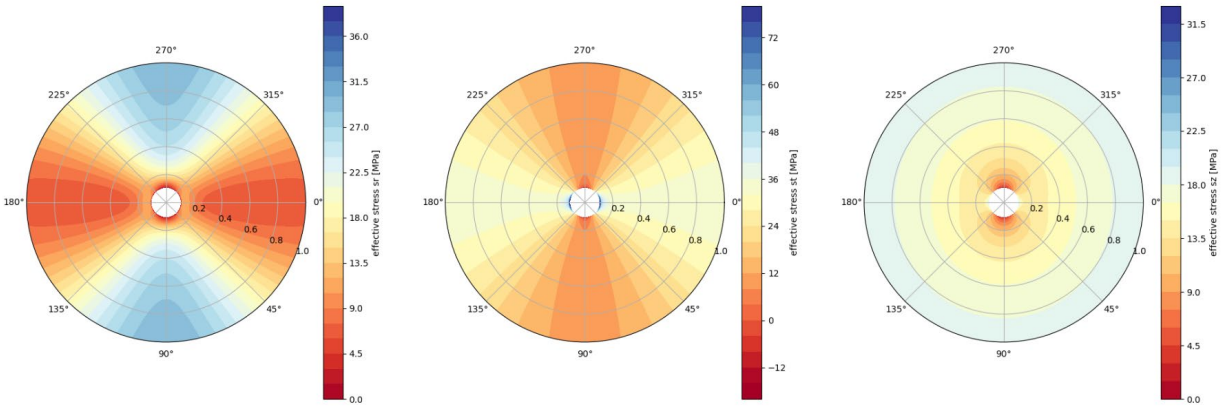

Figure 13 Well bore stability: predicted total effective radial σ_{rr}, tangential $\sigma_{\theta\theta}$ and along hole stress σ_{zz} in polar plots. The 0° orientations correspond to horizontal. Up to 1 meter radius around the borehole, after 120 months of circulation.

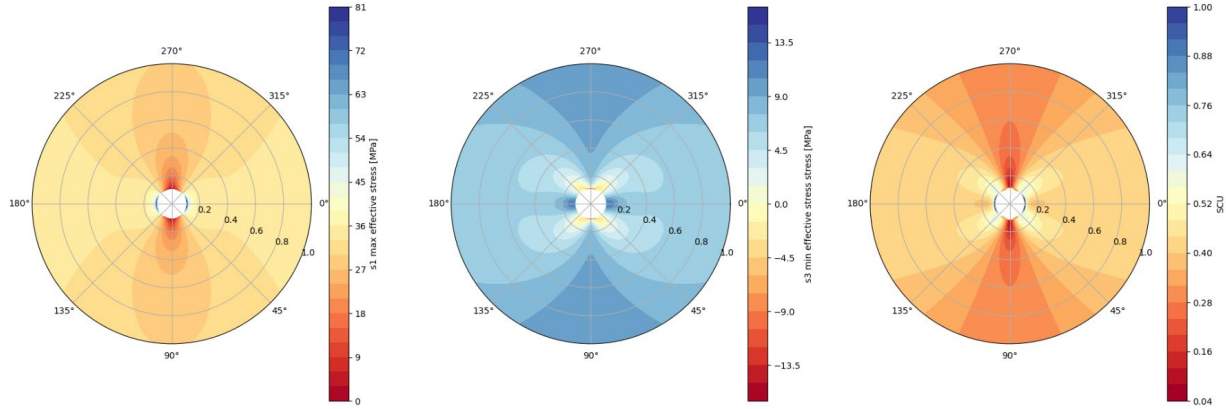

Figure 14 Well bore stability: predicted total largest (s1) and minimum effective stress (s3) and the Shear Capacity Utilization for a cohesion of 20 MPa. Please note that the SCU cannot be used for tensile failure marked by tensile strength which can be significantly lower than the Cohesion or Unconfined Compressive Strength. Up to 1 meter radius around the borehole, after 120 months of circulation.

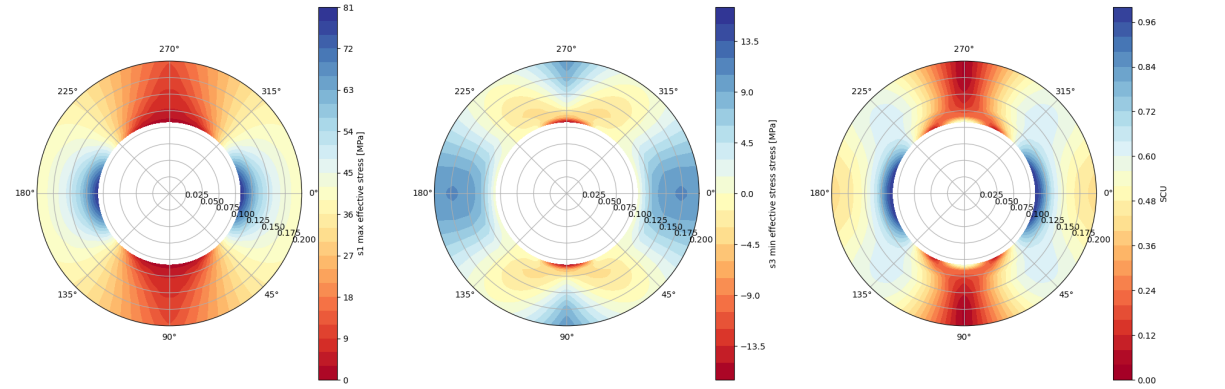

Figure 15 Well bore stability: zoom-in on predicted total largest (s1) and minimum effective stress (s3) and the Shear Capacity Utilization for a cohesion of 20 MPa. Please note that the SCU does not hold for tensile failure marked by tensile strength which can be significantly lower than the Cohesion or Unconfined Compressive Strength. Up to 0.2 meter radius around the borehole, after 120 months of circulation.

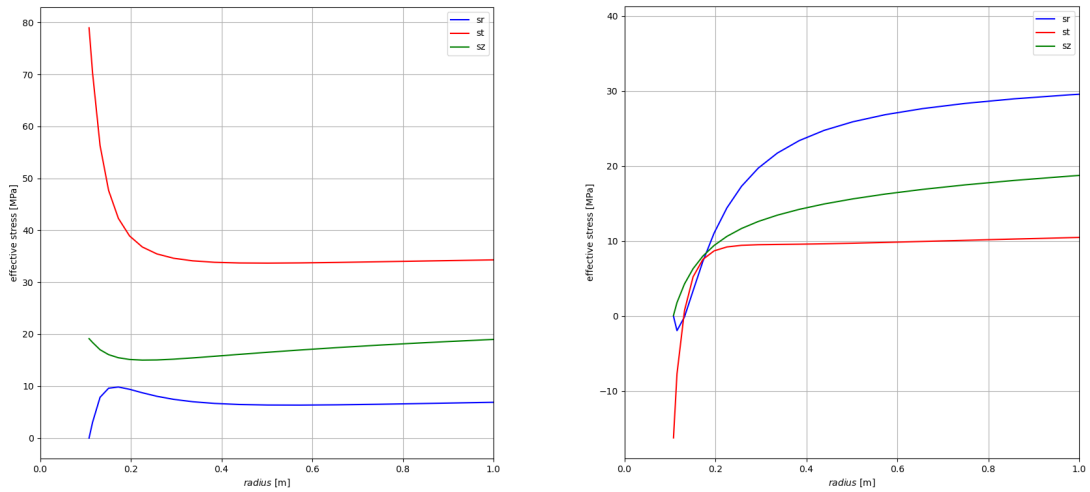

Figure 16 Well bore stability: predicted total effective radial σ_{rr}, tangential $\sigma_{\theta\theta}$ and along hole stress σ_{zz} in (left) azimuth 0° and (right) azimuth 90°. Up to 1 meter radius around the borehole, after 120 months of circulation.

As can be seen in Figure 15 and Figure 16 the borehole wall is stable, except for less than 1 cm of the wall, marked by SCU close to or slightly exceeding 1 (in horizontal direction) and strong tensile stresses of -14 MPa (in vertical direction). According to the Cohesion of the reservoir rock as determined by lab experiments (Table 1) the Shear Capacity Utilization, which takes into account the regional stress field characteristics and Cohesion (Buijze et al., 2017) would remain below 1, except the first few mm at the borehole wall in horizontal direction, indicating shear stability of the borehole. However, the ca -14 MPa tensile stress will most likely lead to fracturing due to tensile failure.

The likelihood for tensile failure is dependent on the actual tensile strength which was not measured in the lab experiments as described in the WP1 results but can be estimated from Cohesion values. For comparison, Berea Sandstone has a Young's Modulus of 10 GPA, cohesion of 11 MPa, friction of 33 deg and porosity of 25%. The Brazilian tests return a tensile strength of 1.7 MPa. For the Triassic drilled in Tilburg, it is likely that the tensile strength will be significantly higher than Berea Sand due to its lower porosity and higher Young's Modulus, but it may not be higher than 3-6 MPa. Therefore, it will create tensile cracks under these conditions. However, these will be limited to the first few mm up to ca 1 cm of the borehole wall. In the analysis we did not consider the impact of Eavor's proprietary Rock-Pipe, which will be placed on the walls of the open hole laterals to seal off the formation from the fluids inside the EL. This could change the rock parameters at the wellbore face, and can to some extent affect the cohesion, friction, and tensile strength.

Please note that the thermal effects responsible for the tensile fractures will manifest themselves very early in the Eavor Loop lifetime, possibly already during drilling when mud circulation is causing borehole wall cooling. The fractures can therefore already occur during the drilling process. Stress effects of thermal cooling do not noticeably increase over time after the first month of weeks of operation. This is clearly demonstrated in Figure 17 and Figure 18, showing the stress effects after one month of circulation, and in comparison to Figure 15 and Figure 16 respectively show hardly any changes. Consequently, the breaching of Rock-Pipe, after the first month of operation is unlikely, and prevention of leakage can be enhanced by deliberately generating thermal stress effects during drilling promoting potential fractures. The early use of Lost Circulations Material (LCM) and Rock-Pipe to plug the crack tip can prevent further propagation. Rock-Pipe can be reapplied throughout the life of the Eavor-Loop. In addition, Eavor can carefully design drilling and operating pressures and circulating fluid densities so as to not exceed the fracture gradient throughout the life of the Eavor-Loop.

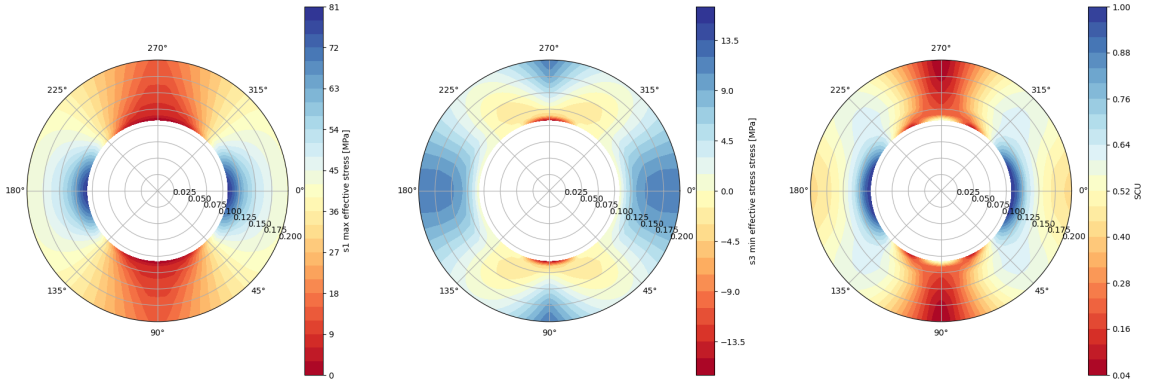

Figure 17 Well bore stability: predicted total largest (s1) and minimum effective stress (s3) and the Shear Capacity Utilization for a cohesion of 20 MPa. Please note that the SCU does not hold for tensile failure marked by tensile strength which can be significantly lower than the Cohesion or Unconfined Compressive Strength. Up to 0.2 meter radius around the borehole, after 1 month of circulation.

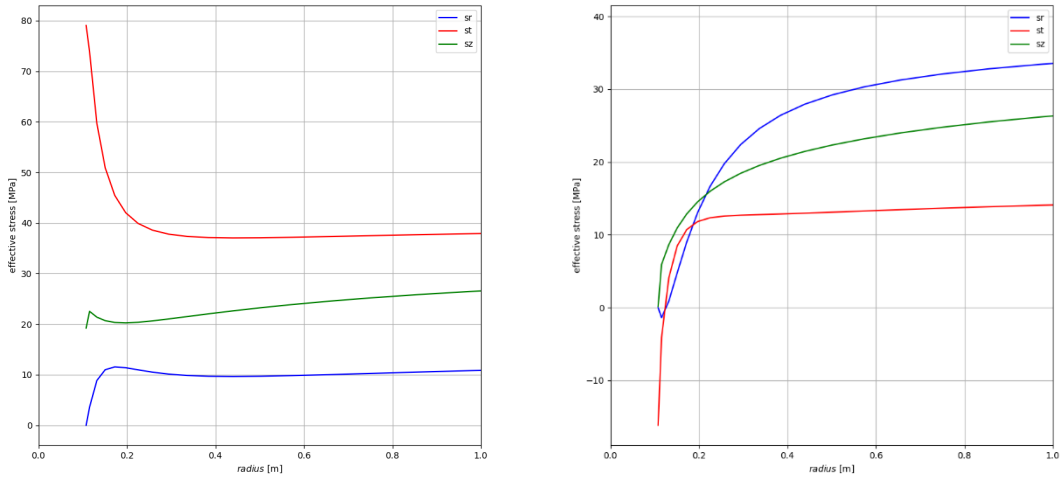

Figure 18 Well bore stability: predicted total effective radial σ_{rr}, tangential $\sigma_{\theta\theta}$ and along hole stress σ_{zz} in (left) azimuth 0° and (right) azimuth 90°. Up to 1 meter radius around the borehole, after 1 month of circulation.

4.2 Reactivation potential of pre-existing faults

Stress effects have been calculated up to 70 meters from the well bore based on the predicted temperature response depicted in Figure 11 at 120 months and have been tested for stability on pre-existing fracture favorably aligned in the (locally rotated) stress field, adopted a cohesion of 0.

The results show Shear Capacity Utilization for pre-existing fractures leading to failure only in the very close vicinity of the borehole (<10 m radius). The associated reactivated fault areas would be relatively small and most likely not result in seismicity which could be felt at surface – unless stress changes are able to trigger theoretically larger events, albeit at much lower probability.

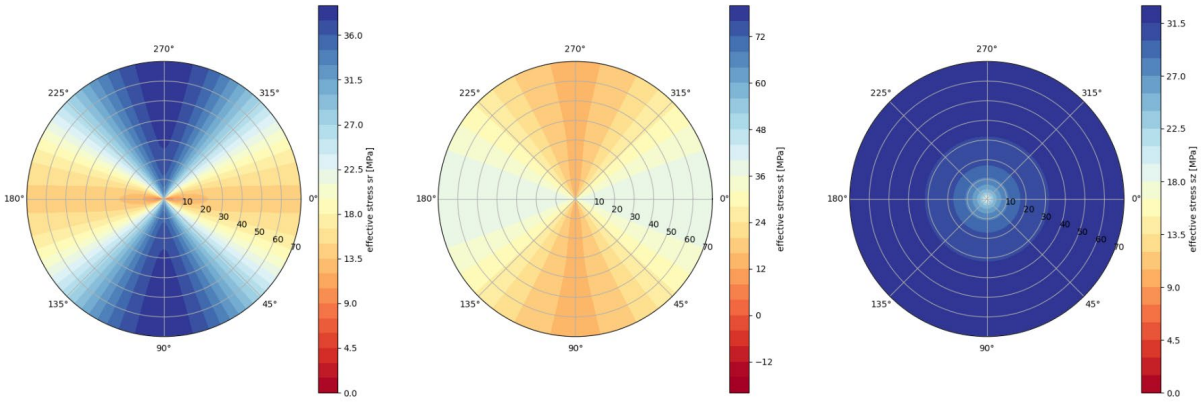

Figure 19 Fault reactivation: predicted total effective radial σ_{rr}, tangential $\sigma_{\theta\theta}$ and along hole stress σ_{zz} in polar plots. The 0 degrees orientations correspond to horizontal. Up to 70 meter radius around the borehole, after 120 months of circulation.

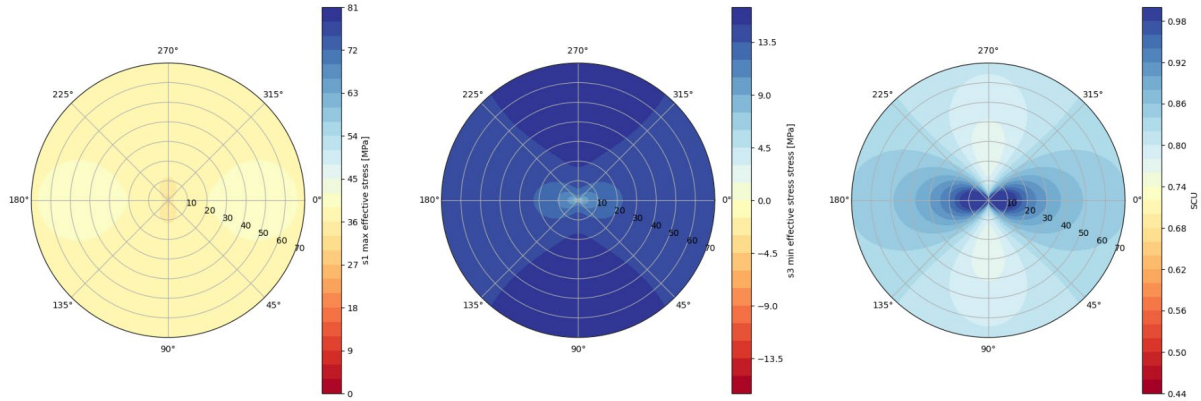

Figure 20 Fault reactivation: predicted total largest (s1) and minimum effective stress (s3) and the Shear Capacity Utilization for a cohesion of 0 MPa. Up to 70 meter radius around the borehole, after 120 months of circulation.

4.3 Sensitivity to in-situ stress

Here we modify the minimum horizontal stress to a slightly higher value 17 MPa/km instead of 15 MPa/km. The effects are shown in the figures.

It is clear that the stresses are more stable, both in terms of tensile stresses at the borehole wall (Figure 21 as well as SCU for fault reactivation (Figure 22). The following models were run assuming 120 months of circulation (Figure 11).

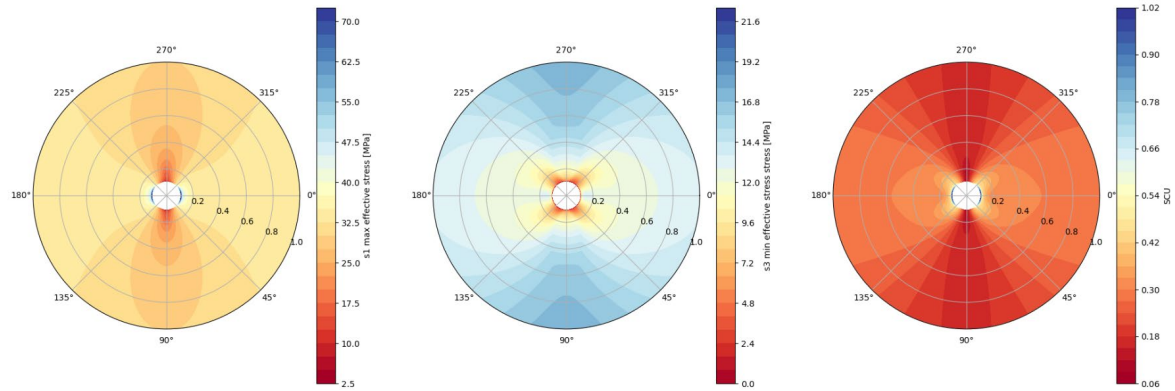

Figure 21 Well bore stability sensitivity to in-situ stress: predicted total largest (s1) and minimum effective stress (s3) and the Shear Capacity Utilization for a cohesion of 20 MPa up to a radius of 1 m Up to 1 meter radius around the borehole, after 120 months of circulation.

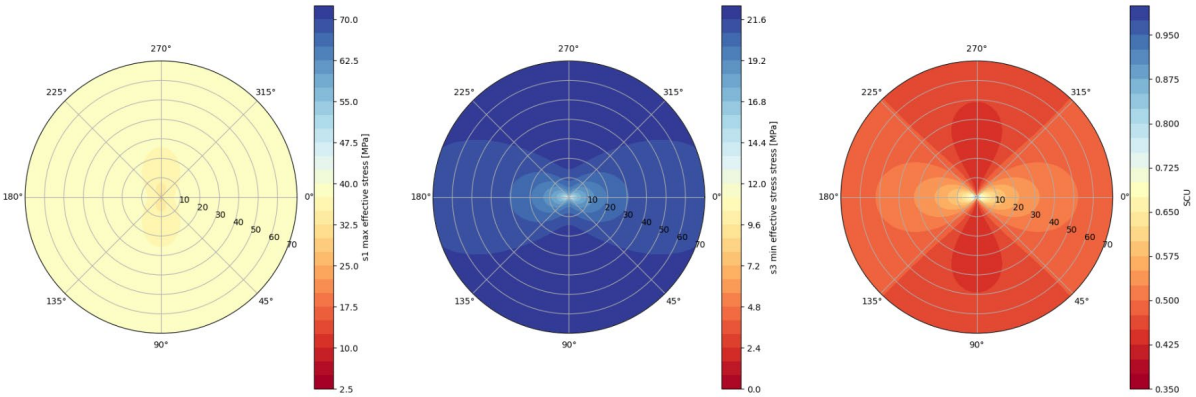

Figure 22 Fault reactivation sensitivity to in-situ stress: predicted total largest (s1) and minimum effective stress (s3) and the Shear Capacity Utilization for a cohesion of 0 MPa. Up to a radius of 70 m, after 120 months of circulation.

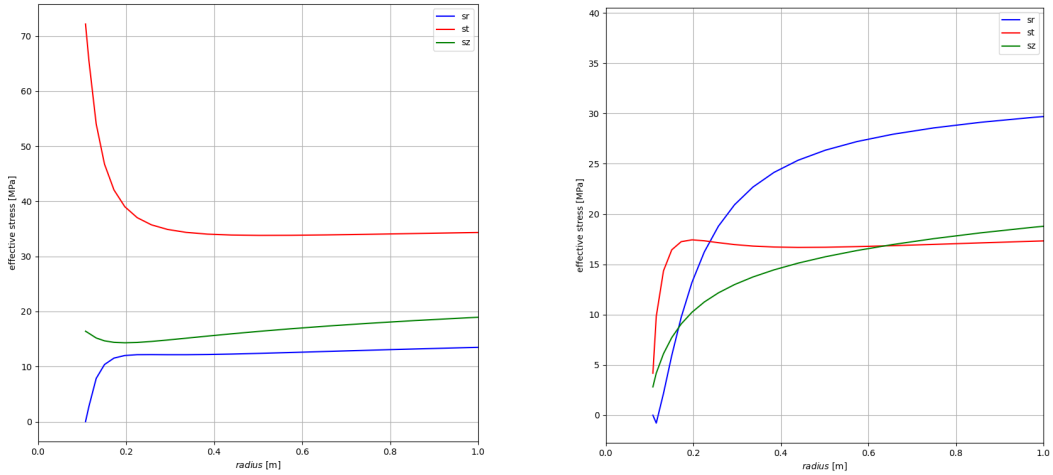

Figure 23 Well bore stability sensitivity to in-situ stress: predicted total effective radial σ_{rr}, tangential $\sigma_{\theta\theta}$ and along hole stress σ_{zz} in (left) azimuth 0° and (right) azimuth 90°. Up to 1 meter radius around the borehole, after 120 months of circulation.

4.4 Sensitivity to friction angle

The sensitivity to fault reactivation has been analyzed for a more conservative (higher) estimate of the friction angle (in line with the range given in Table 1. This results in reduced SCU values, preventing shear failure for existing faults (Figure 25). Well bore stability is still prone to high tensile stresses (Figure 24). The following models were running assuming 120 months of circulation (Figure 11).

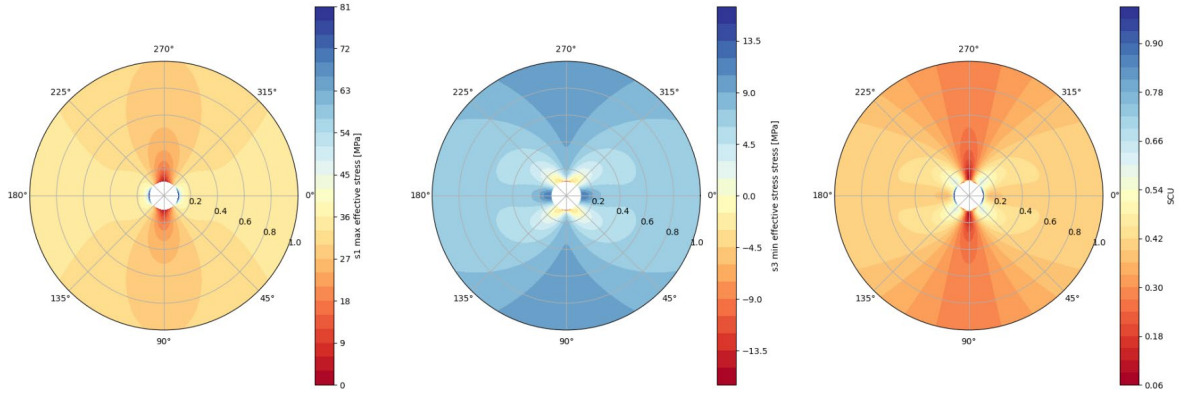

Figure 24 Well bore stability sensitivity to friction angle: predicted total largest (s1) and minimum effective stress (s3) and the Shear Capacity Utilization for a cohesion of 20 MPa. Up to a radius of 1 m, for 120 months of circulation.

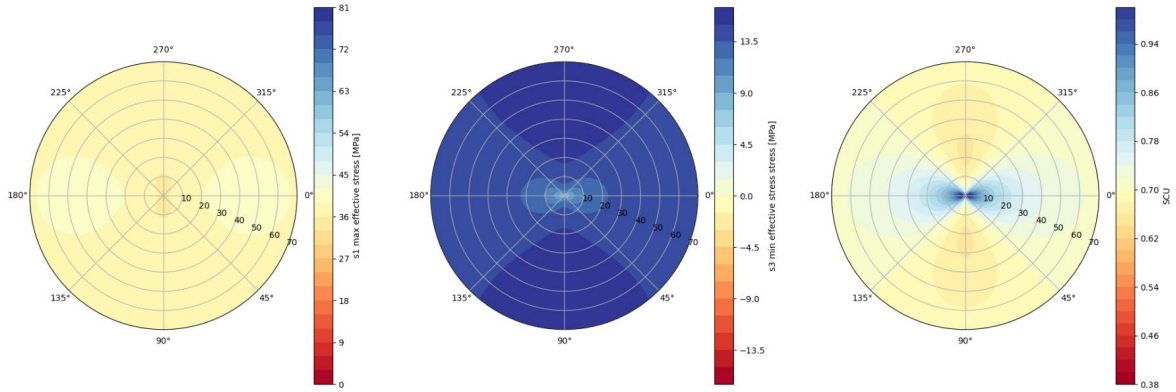

Figure 25 Fault reactivation sensitivity to friction angle: predicted total largest (s1) and minimum effective stress (s3) and the Shear Capacity Utilization for a cohesion of 0 MPa. Up to a radius of 70 m, for 120 months of circulation.

4.5 Sensitivity for injection temperature

Lower injection temperature will result in larger cooling of the well bore, in particular at the bore hole wall. In order to test the sensitivity to lower injection temperature the injection temperature was reduced from 60°C to 40°C. As demonstrated in Figure 27, Figure 28, and Figure 29, the amplitude of the stress changes is enlarged and results in more accentuated bore hole tensile failure instabilities and a potentially larger instable zone for frictional reactivation of pre-existing faults, further away from the borehole. However, compressional borehole breakouts become less likely with a lower injection temperature. The following models were running assuming 120 months of circulation (Figure 11).

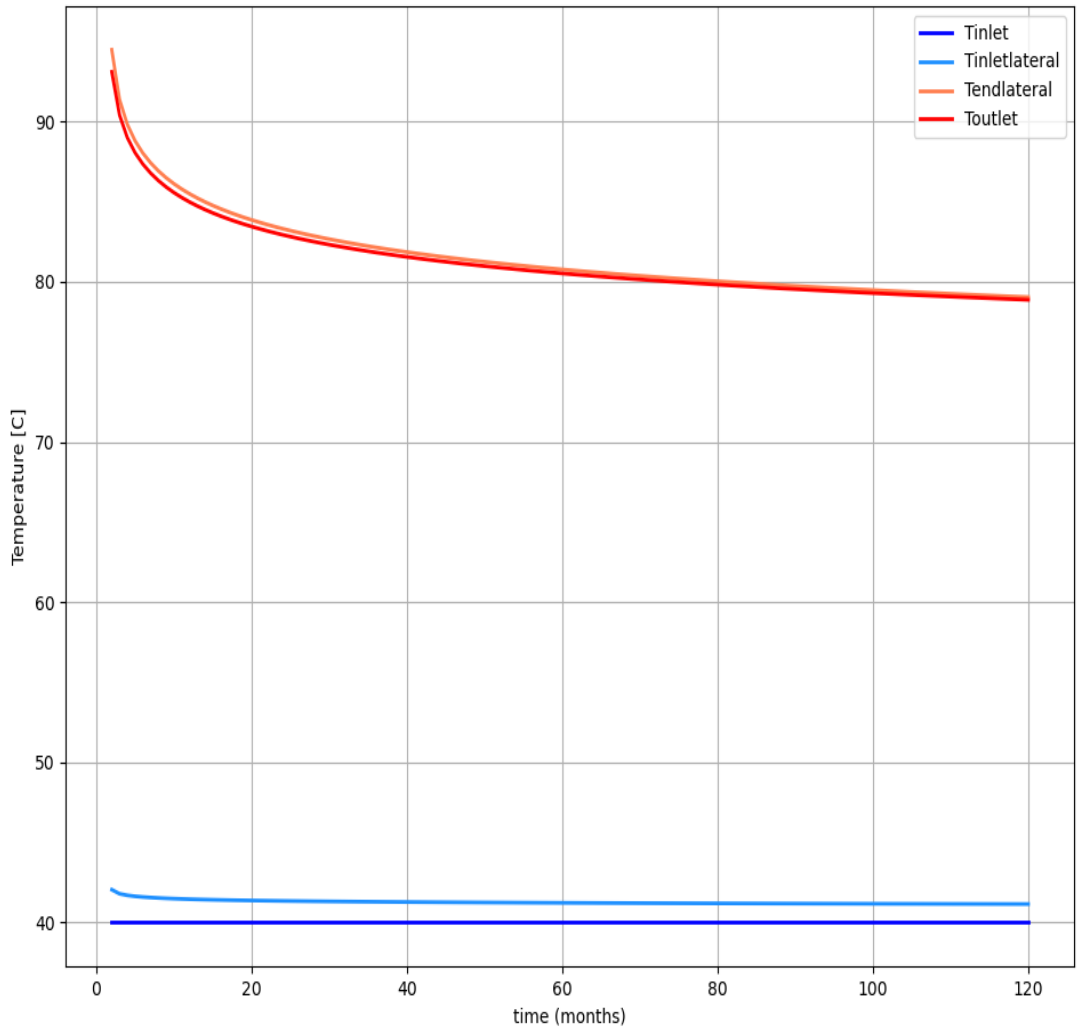

Figure 26 Thermal response of the Tilburg Eavor Loop at an injection temperature of 40C.

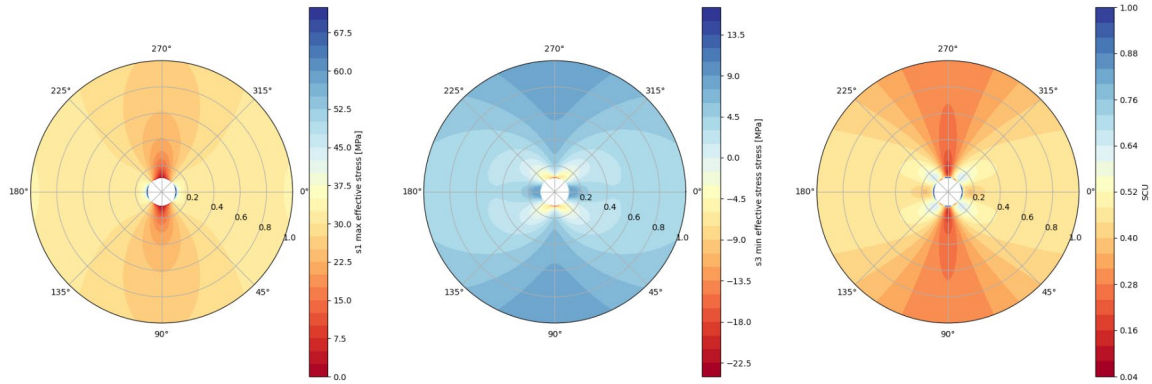

Figure 27 predicted total largest (s1) and minimum effective stress (s3) and the Shear Capacity Utilization for a cohesion of 20 MPa up to a radius of 1 m

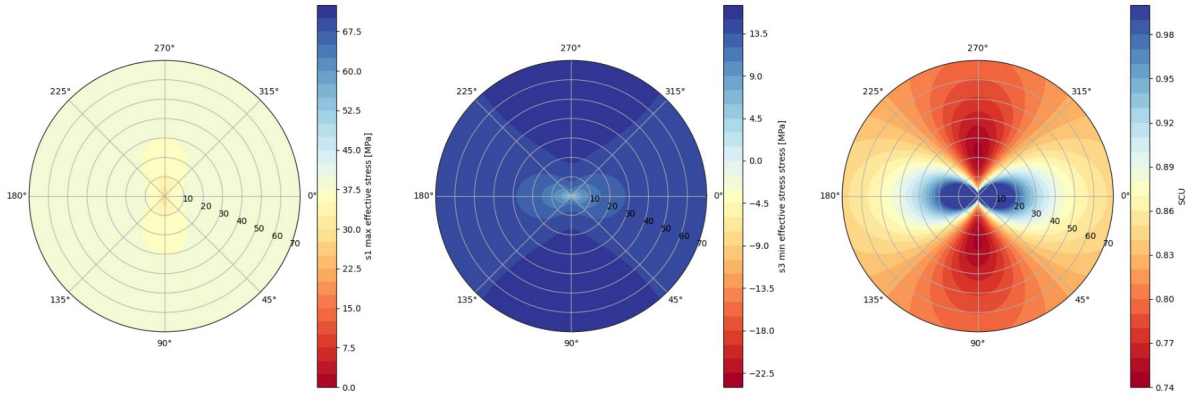

Figure 28 predicted total largest (s1) and minimum effective stress (s3) and the Shear Capacity Utilization for a cohesion of 0 MPa, up to a radius of 70 m

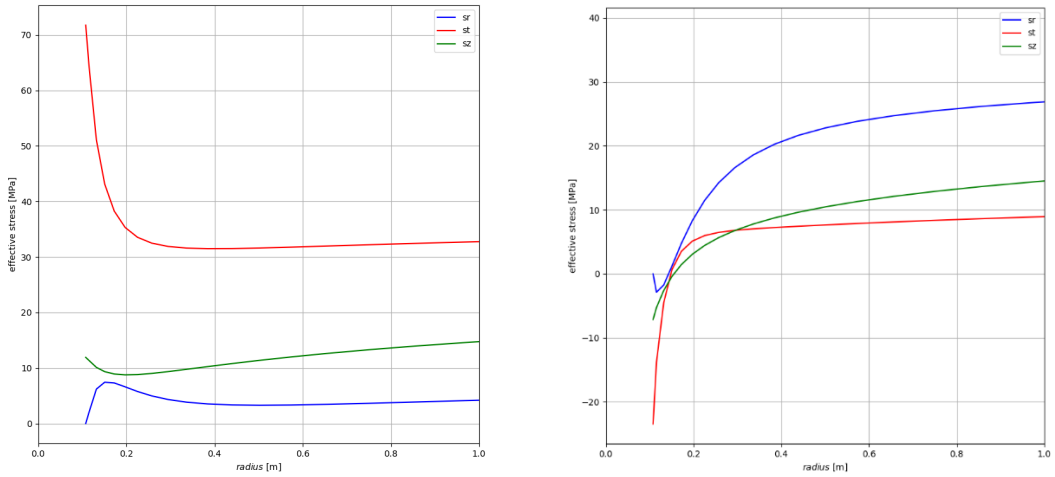

Figure 29 predicted total effective radial σ_{rr}, tangential $\sigma_{\theta\theta}$ and along hole stress σ_{zz} in (left) azimuth 0 and (right) azimuth 90. (Up to 1 meter radius around the borehole).

5 CO_2 footprint and LCA

The basis for the analysis in this report is the recent study on LCA (Life Cycle Assessment) and underlying carbon footprint performed in the framework of WarmingUP (Dinkelman et al., 2021) for conventional geothermal doublet systems. In this study the CO_2 emissions per unit energy produced have been subdivided into 3 phases (construction, operation and decommissioning, Figure 30).

An LCA results in an overview of the total environmental impact of a product or system throughout its life cycle. The methodology expresses the total environmental impact into three categories, also called areas of protection (endpoint area of protection):

1. Human Health (expressed in DALYs: disability adjusted life years).

2. Ecosystems (expressed in species loss per year).

3. Resource availability (expressed monetarily in $)

The LCA analysis first analyzes which so-called impact categories contribute to these three categories. The model tracks certain relationships between all of these impact categories (midpoint impact category) and how they manifest themselves via different damage pathways to the three protection areas. The results for conventional geothermal doublets show that the main impact categories for geothermal energy are global warming, particulate matter formation, formation of ozone, soil acidification, land use, and scarcity of fossil resources. The most important impact category is 'global warming'. This contributes about 80% to the protection areas Human Health and Ecosystems. In the category Commodities, 'scarcity of fossil resources' is the main impact category (see Dinkelman et al., 2021). For the Eavor-Loop the same main categories apply.

Next, the LCA analyzes the relative contribution of the different phases of the geothermal life cycle in more detail. Figure 30 shows the impact on global warming for each phase of a conventional doublet in terms of the CO_2 emissions (Dinkelman et al., 2021). Of the three phases, the operational phase has by far the largest impact on global warming (9.9 kg CO_2/GJ). The impact of the construction phase is significantly lower at 0.27 kg CO_2/GJ. The decommissioning phase contributes relatively little to this impact category (0.03% of the total). Based on these results, the main messages are:

1. The environmental impact of a geothermal plant primarily impacts global warming

2. This impact occurs mainly during the use phase (~97%).

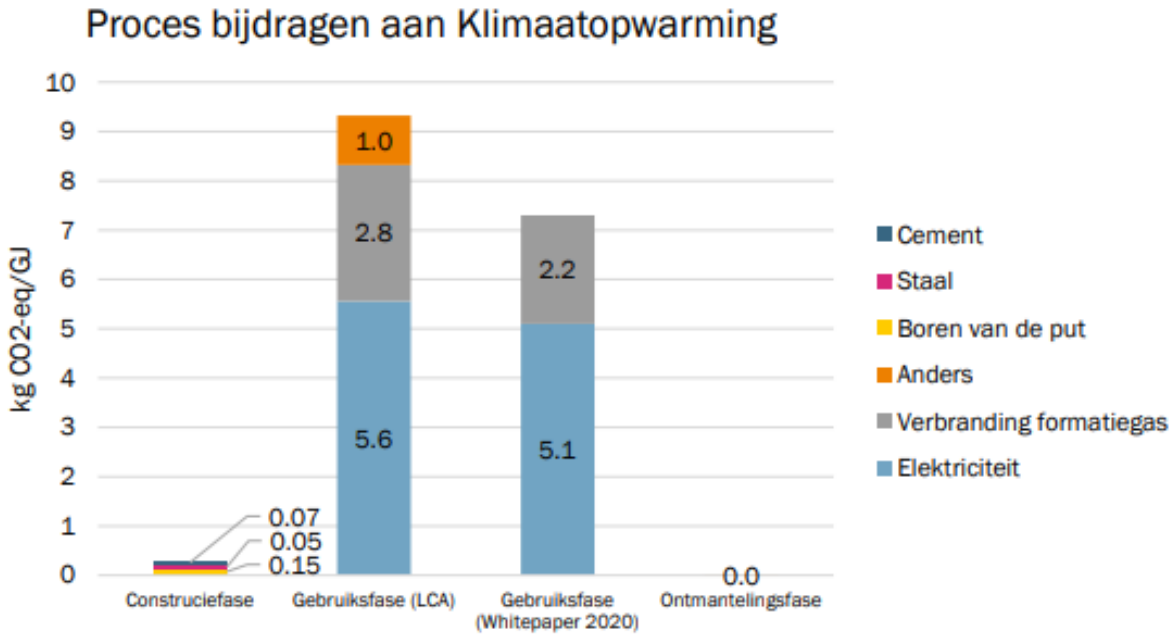

Figure 30 CO_2 emissions (kg CO_2-eq/GJ) for the different phases of a conventional geothermal doublet: construction phase, operational phase (gebruiksfase), and abandonment phase (ontmantelingsfase). Construction phase emissions relate to drilling (boren), cementing and steel (staal) completion. Operational emissions include power consumption (elektriciteit) for driving the ESP and the burning of formation gas (formatiegas). Source: Dinkelman et al., 2021.

The CO_2 footprint of the Eavor-Loop has been analyzed in view of a conventional geothermal doublet system for the three phases of development (cf Figure 30):

Construction: The construction of an Eavor-Loop with ca 12 laterals is marked by significantly higher emissions than a conventional doublet due to much longer borehole trajectory to be drilled, attributed to the laterals, and the slightly deeper target over 3000m depth, compared to ca 2200 m for conventional doublet systems. The laterals are not cemented or cased resulting in ca 1.5 kg CO_2-eq/GJ. A 50% deeper depth of the vertical trajectories would lead to another addition of ca 0.13 kg CO_2-eq/GJ. Consequently, the construction phase emissions are expected to be responsible for at most 2 kg CO_2-eq/GJ increase relative to a conventional doublet.

Operation: The fluid circulation for the Eavor-Loop requires significantly less pumping power compared to a conventional depth. For the Tilburg Eavor-Loop, marked by a pumped pressure of 2 MPa, the power consumption to drive the Eavor-Loop is ca 2.5% of the thermal power produced. The related CO_2-eq/GJ is about half of the emissions related to a conventional geothermal doublet, resulting in a saving of at least 2 kg CO_2-eq/GJ. In addition, the Eavor-Loop has no formation gas in the produced fluids, resulting in no emissions related to burning of formation gas, saving over 2 kg CO_2-eq/GJ.

Decommissioning: for decommissioning the activities and materials used are comparable for conventional geothermal, related to plugging the vertical trajectories, and assumed to produce negligible CO_2 emissions.

In summary, the emission characteristics (kg CO_2-eq/GJ) of the Eavor-Loop are ca 20% improved compared to a conventional geothermal doublet system, saving over 2 kg CO_2-eq/GJ. In more detail,

emission related to construction is slightly higher than a conventional doublet, related to much longer drilled sections. However, the operation related emissions marked by reduced pumping power and absence of formation gas compared to a conventional doublet system, and offset the increase related to construction.

6 Conclusions & Discussion

Thermal performance

- In the Tilburg area the considered Eavor-Loop is a so-called James Joyce chain design targeting the Triassic sandstones at ca 3200 m depth with 12 laterals. The layout of the wells is based on key well survey points which have been defined by Eavor. For the operation of the Eavor Loop it is assumed that inlet temperatures will be ~60°C and flow rate of 60 kg/s with the assumption that the water density at 60°C is 1000 kg/s.
- The thermal model introduced in section Appendix A has been used to calculate the thermal response of the Eavor Loop for 10 years at constant flow rate conditions. The grid sizes in radial direction have been chosen such that the logarithmic value of the cell centers radial coordinates is linearly increasing from sub cm-size at the well bore to meter size at a radial distance of 70 m, which is sufficient to fully cover the transient heat flow over the simulated lifetime.
- The predicted thermal power is in excess of 7 MWth.
- The Eavor Loop has a long lifetime marked by a very moderate linear decline of the production temperature and power over a lifetime of 10s of years, with minor thermal interference of laterals if placed with a spacing of ca 70 m.

Borehole stability:

- The borehole wall upon cooling of the Eavor-Loop is stable, except for less than 1 cm of the wall at the entry of the laterals, marked by a Shear Capacity Utilization (SCU) close to or slightly exceeding 1 indicative for frictional instability (in horizontal direction) and strong tensile stresses of -14 MPa (in vertical direction). According to the Cohesion of the reservoir rock as determined by lab experiments (Table 1) the SCU, which takes into account the regional stress field characteristics and Cohesion, would remain below 1, except the first few mm at the borehole wall in horizontal direction, indicating shear stability of the borehole. However, the ca 14 MPa tensile stress will most likely lead to fracturing due to tensile failure.
- The likelihood for tensile failure is dependent on the actual tensile strength which was not measured in the lab experiments as described in the WP1 results but can be estimated from Cohesion values. For the Triassic drilled in Tilburg, cohesion may not be higher than 3-6 MPa. Therefore, it will create tensile cracks under the ca 14Mpa tensile stress. However, these will be limited to the first few mm up to ca 1 cm of the borehole wall. In the analysis we did not consider the impact of Eavor's proprietary Rock-Pipe, which will be placed on the walls of the open hole laterals to seal off the formation from the fluids inside the EL. This could change the rock parameters at the wellbore face, and can to some extent affect the cohesion, friction, and tensile strength.
- The thermal effects, responsible for the tensile fractures will manifest themselves very early in the Eavor-Loop lifetime, possibly already during drilling when mud circulation is causing borehole wall cooling. The fractures can therefore already occur during the drilling process. Stress effects of thermal cooling do not noticeably increase over time after the first month of weeks of operation. Consequently, the breaching of Rock-Pipe, after the first month of operation is unlikely, and prevention of leakage can be enhanced by deliberately generating thermal stress effects during drilling promoting potential fractures. The early use of Lost Circulations Material (LCM) and Rock-Pipe to plug the crack tip can prevent further propagation. Rock-Pipe can be reapplied throughout the life of the Eavor-Loop. In addition, Eavor can carefully design drilling and operating pressures

and circulating fluid densities so as to not exceed the fracture gradient throughout the life of the Eavor-Loop.

Potential reactivation of faults:

- Stress effects have been calculated up to 70 meters from the well bore based on the predicted temperature response at 120 months and have been tested for stability on pre-existing fracture favorably aligned in the (locally rotated) stress field, adopted a cohesion of 0.
- The results show Shear Capacity Utilization (SCU) for pre-existing fractures leading to failure only in the very close vicinity of the borehole (<10 m radius). The associated reactivated fault areas would be relatively small and most likely not result in seismicity which could be felt at surface – unless stress changes are able to trigger theoretically larger events, albeit at much lower probability.

Sensitivities:

- The results for potential fault reactivation are very sensitive to the in-situ stress assumptions. Adopting more a higher horizontal stress gradient of 17 MPa/km instead of the base case 15 MPa/km, results in more stable predictions, both in terms of SCU for fault reactivation, as well as tensile stresses at the bore hole wall, positively affecting borehole stability.
- The sensitivity to fault reactivation has been analyzed for a higher estimate of the friction angle of pre-existing faults (in line with the range given in Table 1). This results in reduced SCU values, preventing shear failure for existing faults. Well bore stability is still prone to high tensile stresses.
- Lower injection temperature will result in larger cooling of the well bore, in particular at the bore hole wall. In order to test the sensitivity to lower injection temperature the injection temperature was reduced from 60°C to 40°C. Consequently, the amplitude of the stress changes is enlarged and results in more accentuated bore-hole instabilities and a potentially larger instable zone for frictional reactivation of pre-existing faults, further away from the borehole.

CO_2 footprint:

- The emission characteristics (kg CO_2-eq/GJ) of the Eavor-Loop are ca 20% improved compared to a conventional geothermal doublet system, saving over 2 kg CO_2-eq/GJ. In more detail, emission related to construction is slightly higher than a conventional doublet, related to much longer drilled sections. However, the operation related emissions marked by reduced pumping power and absence of formation gas compared to a conventional doublet system, and offset the increase related to construction.

7 References:

Aadnoy, B.S., 1988. Modelling of the Stability of Highly Inclined Boreholes in Anisotropic Rock formations. SPE Drilling and Engineering, sep. 1988, 259-268. SPE 16526.

Aadnoy, B.S., Chenevert, M.E., 1987. Stability of Highly Inclined Boreholes. SPE Drilling and Engineering, dec 1987, 364-374. SPE 16052

Beckers, K.F., Johnston, H.E., 2022. Techno-economic performance of Eavor-Loop 2.0. PROCEEDINGS, 47 th Workshop on Geothermal Reservoir Engineering. Stanford University, Stanford, California, February 7-9, 2022, SGP-TR-223

Buijze, L., Van den Bogert, P.A.J., Wassing, B.T.T., Orlic, B., Ten Veen. J., 2017. Fault reactivation mechanisms and dynamic rupture modelling of depletion-induced seismic events in a Rotliegend gas reservoir.

Dinkelman, D., Dijkstra, H., De Simon, L., Ros, J., Hanegraaf, M., Veldkamp, H., Van Wees, 2021. Duurzaamheid Geothermie factsheet, https://www.tno.nl/publish/pages/2137/tno-2021-duurzaamheid.pdf

Droniou, J., 2013. Finite volume schemes for diffusion equations: introduction to and review of modern methods, <hal-00813613v1>

Gies, C., Struijk, M., Békési, E., Veldkamp, H., van Wees, J.D., 2021. An effective method for paleo-temperature correction of 3D thermal models: A demonstration based on high resolution datasets in the Netherlands, Global and Planetary Change, https://doi.org/10.1016/j.gloplacha.2021.103445

Holmes et al., 2021; Multilateral-closed-loop-geothermal-systems-as-a-ZELFR.pdf (eavor.com)

Nguyen, D., Miska, S., Yu, M., 2009. Modelling Thermal Effects on Wellbore Stability. SPE paper 133428

Tang, L., and Luo, P., 1998. The Effect of the Thermal Stress on Wellbore Stability. SPE paper 39505

Van Wees, 2021. Audit Report Eavor Loop. TNO - Eavor-Loop™ Audit Report - Eavor

Appendix A. Thermal simulation

The thermal changes for the Eavor-Loop can be simulated with a radial symmetric simulation approach around the borehole. Various solution techniques exist either based on semi-analytical approaches (Van Wees,2021, Beckers et al., 2022) solving temperature changes in the borehole, or numerical formulations which solve the full temperature field surrounding the borehole (Holmes et al., 2021). Here we adopt the latter approximated by a Finite volume formulation.

A.1. Finite volume formulation

The thermal field is solved with a finite volume finite difference formulation. The finite volume method solves for a potential u_K (e.g., temperature, pressure) at the center of polyhedral cell (index K) at the center point $\boldsymbol{x}_K$, based on continuity equations taking into account the fluxes at the interfaces to other cells (Droniou, 2013; Figure 31).

$$\frac{dU_K}{dt} = \frac{1}{c_K}\left(\nabla.\mathbf{K}\nabla u_K + \mathrm{q}_K\right) \qquad (1)$$

Which can be written in the finite volume formulation with V is volume of the cell

$$\frac{dU_K}{dt} = \frac{1}{Vc_K}\left(\sum \mathrm{A}_\sigma \mathrm{n}_\sigma.\boldsymbol{\kappa_K}\nabla u_K + \mathrm{Q}_K\right) \qquad (2)$$

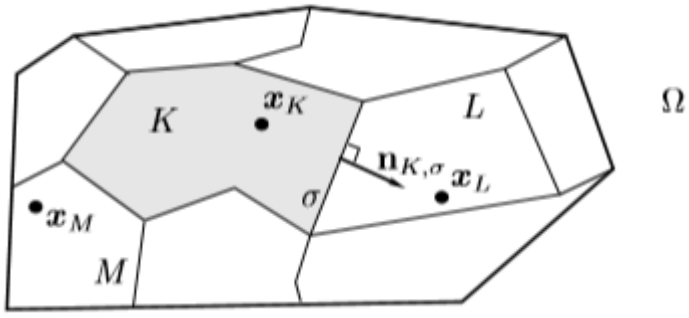

Figure 31 Finite volume formulation for Cell K, constructed from fluxes from the polyhedral faces σ

A.2. Axisymmetric heat conduction formulation

For a 2D radial symmetry we can write for the heat diffusion in radial dimension (in Section 2.3 we will complement the radial conduction with lateral conduction):

$$\frac{dT_j}{dt} = \frac{1}{Vc_j}\left(CR_{j-\frac{1}{2}}(T_{j-1} - T_j) + CR_{j+\frac{1}{2}}(T_{j+1} - T_j)\right) \qquad (3)$$

Where T is temperature of cell j, Vc_j is the product of the volumetric heat capacity (J m^{-3} K^{-1}) and the volume of cell j., $CR_{j-\frac{1}{2}}$ and $CR_{j+\frac{1}{2}}$ are the conductance values connecting the cells (j ,j-1) and connecting (j, j+1) respectively, and are defined (Langevin, 2008) as:

$$CR_{j+\frac{1}{2}} = \frac{2\,\pi\ K_r\,\Delta z}{\ln(\frac{r_{j+1}}{r_j})} \qquad (4)$$

Where K_r is the radial conductivity of the cells j and j+1. If $K_{r,j+1}$ is not equal to $K_{r,j}$ we write:

$$CR_{j+\frac{1}{2}} = \frac{2\,\pi\ \ \Delta z}{\ln(\frac{r_{j+1}}{r_{j+\frac{1}{2}}})\frac{1}{K_{r,j+1}}+\ln(\frac{r_{j+\frac{1}{2}}}{r_j})\frac{1}{K_{r,j}}} \qquad (5)$$

In an implicit solution scheme for the temperature at moving from timestep n to n+1 we can write:

$$\frac{dT_j}{dt} = \frac{T_j^{n+1}-T_j^n}{\Delta t} = \frac{1}{Vc_j}\left(CR_{j-\frac{1}{2}}\left({T_{j-1}}^{n+1} - {T_j}^{n+1}\right)+CR_{j+\frac{1}{2}}\left(({T_{j+1}}^{n+1} - {T_j}^{n+1})\right)\right) \qquad (6)$$

$${T_j}^{n+1} = \Delta t\frac{1}{Vc_j}\left(CR_{j-\frac{1}{2}}\left({T_{j-1}}^{n+1} - {T_j}^{n+1}\right)+ CR_{j+\frac{1}{2}}\left(({T_{j+1}}^{n+1} - {T_j}^{n+1})\right)\right) + {T_j}^{n} \qquad (7)$$

Where Δt is the timestep in seconds., and can written as:

$$\left(1 + \Delta t\frac{1}{Vc_j}\left(CR_{j-\frac{1}{2}} + CR_{j+\frac{1}{2}}\right)\right){T_j}^{n+1} - \Delta t\frac{1}{Vc_j}\left(CR_{j-\frac{1}{2}}\,{T_{j-1}}^{n+1} + CR_{j+\frac{1}{2}}{T_{j+1}}^{n+1}\right) = {T_j}^{n} \qquad (8)$$

For middle nodes we can write, by multiplying both sides by $\frac{Vc_j}{\Delta t}$:

$$\left(\frac{Vc_j}{\Delta t} + CR_{j-\frac{1}{2}} + CR_{j+\frac{1}{2}}\right){T_j}^{n+1} - \ CR_{j-\frac{1}{2}}\,{T_{j-1}}^{n+1} - CR_{j+\frac{1}{2}}{T_{j+1}}^{n+1} = \frac{Vc_j}{\Delta t}\ \ {T_j}^{n} \qquad (9)$$

For the last node, j =nr, we assume zero heat flow

$$\left(\frac{Vc_j}{\Delta t} + CR_{j-\frac{1}{2}}\right){T_j}^{n+1} - CR_{j-\frac{1}{2}}{T_{j-1}}^{n+1} = \frac{Vc_j}{\Delta t}\ \ {T_j}^{n} \qquad (10)$$

A.3. Mass flow

The first cell (j=0) corresponds to the well bore marked by fluid flow. The lateral heat transfer within the well bore $K_{r,0}$ is assumed to be marked by a very high conduction value (set to 30) to mimic effective fluid mixing. For the first node (j=0) we include the mass flow rate for thermal advection

along the well bore from cell (0,i-1), where I denotes the along axis position in the Eavor loop. Index i=0 corresponds to the injection point of the Eavor loop:

$$\frac{dT_0}{dt} = \frac{1}{Vc_0}\left(CR_{\frac{1}{2}}\left({T_1}^{n+1} - {T_0}^{n+1}\right) + \dot{m}\, c_f \left({T_{0,i-1}}^{n+1} - {T_0}^{n+1}\right)\right) \qquad (11)$$

$$\left(1 + \frac{\Delta t}{Vc_0}\ CR_{\frac{1}{2}} + \frac{\Delta t}{Vc_0}\,\dot{m}\, c_f\right) {T_0}^{n+1} - \frac{\Delta t}{Vc_0}\ CR_{\frac{1}{2}}\left({T_1}^{n+1}\right)$$

$$= {T_0}^{n} + \frac{\Delta t}{Vc_0}\,\dot{m}\, c_f \left({T_{0,i-1}}^{n+1}\right)$$

$$\left(1 + \frac{\Delta t}{Vc_0}\left(CR_{\frac{1}{2}} + \dot{m}\, c_f\right)\right) {T_0}^{n+1} - \frac{\Delta t}{Vc_0}\ CR_{\frac{1}{2}}{T_1}^{n+1} = {T_0}^{n} + \frac{\dot{\Delta} t}{Vc_0}\left(\dot{m}\, c_f\, {T_{0,i-1}}^{n+1}\right) \quad (12)$$

Such that we can write:

$$\left(\frac{Vc_0}{\Delta t} + CR_{\frac{1}{2}} + \dot{m}\, c_j\right){T_0}^{n+1} - CR_{\frac{1}{2}}{T_1}^{n+1} = \frac{Vc_0}{\Delta t}\ {T_0}^{n} + \dot{m}\, c_j\ {T_{0,i-1}}^{n+1} \qquad (13)$$

As well as the temperature boundary condition for $T_{0,0}$

$$\left(\frac{Vc_0}{\Delta t} + CR_{\frac{1}{2}} + \dot{m}\, c_j\right){T_{0,0}}^{n+1} - CR_{\frac{1}{2}}{T_{1,0}}^{n+1} = \frac{Vc_0}{\Delta t}\ {T_{0,0}}^{n} + \dot{m}\, c_j\ {T_{inlet}}^{n+1} \quad (14)$$

For the cells in the laterals, we assume that the flow rate is equally distributed along the number of laterals

A.4. Along axis heat conduction

RHS += $\left(CZ_{j,i-\frac{1}{2}}\left({T_{j,i-1}}^{n} - {T_{j,i}}^{n}\right) + CZ_{j,i+\frac{1}{2}}\left(\left({T_{j,i+1}}^{n} - {T_{j,i}}^{n}\right)\right)\right)$

Where:

$$CZ_{j,i-\frac{1}{2}} = \frac{1}{\left(\frac{0.5\ \Delta z_i}{K_{l\,(j,i)}\pi\left({r_{j+\frac{1}{2},i}}^{2} - {r_{j-\frac{1}{2},i}}^{2}\right)} + \frac{0.5\ \Delta z_{i-1}}{K_{l\,(j,i-1)}\pi\left({r_{j+\frac{1}{2},i-1}}^{2} - {r_{j-\frac{1}{2},i-1}}^{2}\right)}\right)}$$

Where $K_{l\,(j,i)}$ is the lateral conductivity of the cell j,i, where i is along hole index

A.5. Heat solution interaction scheme

The heat solution is performed by along hole discretization in segments of ca 100 m length. Time steps are set to 1 day. The surface temperatures outside the well bore are held fixed in the first and last segment of the simulation grid. The inlet temperature of the first segment in the well bore is set equal to the observed/target inlet temperature. The outlet temperature is taken from the penultimate segment in order to avoid strong influence from the constant surface temperature boundary condition. For the laterals it is assumed that each of the laterals takes an equal amount of the mass rate, summing up to the total flowrate, and that each of the laterals has exactly the same along hole length and ambient temperature characteristics. This greatly simplifies the calculations as basically just one loop is modelled.

A.6. Eavor lite evaluation

The thermal solution has been checked against analytical solutions as documented in the TNO-audit report of the EAVOR loop (Van Wees, 2021) and also has been checked for more detailed variations in flow rate, inlet temperatures (Holmes et al., 2021, Figure 32 and Figure 33)

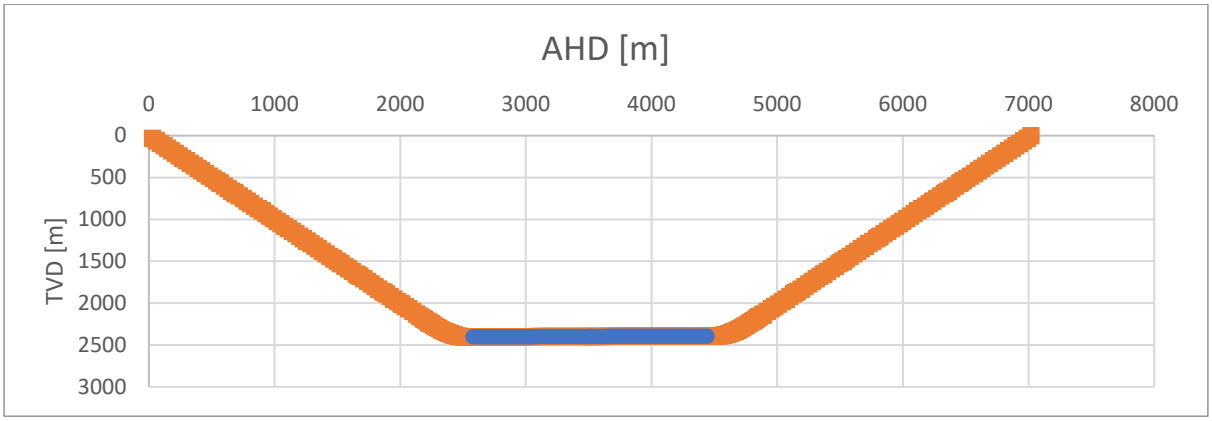

Figure 32 Layout in along axis direction and depth for the Eavor Lite Loop (for more details, Holmes et al, 2021; Van Wees et al., 2021). The lateral section is approximately 1800 m long (blue).

The discretization of the simulation grid is depicted in Table 3 whereas all other parameters have been chosen in accordance with Van Wees, 2021. The grid sizes in radial direction have been chosen such that the logarithmic value of the cell centers radial coordinates is linearly increasing. This results in order cm-size cell radial size of first grid-cells surrounding the wells.

Table 3 Simulation grid parameters for the Eavor Loop Lite Loop

parameter	value	unit
total length	7020	m
number of segments (along hole)	100	
extent of grid in radial direction	70	m
number of grid cells in radial direction	50	
start laterals	2670	m
end laterals	4350	m
number of laterals	2	

The thermal solution allows to evaluate the thermal evolution in the radial dimension as well at position along the well axis. Figure 33 shows the evolution of temperature over time for the Eavor Loop Lite at different positions along the loop.

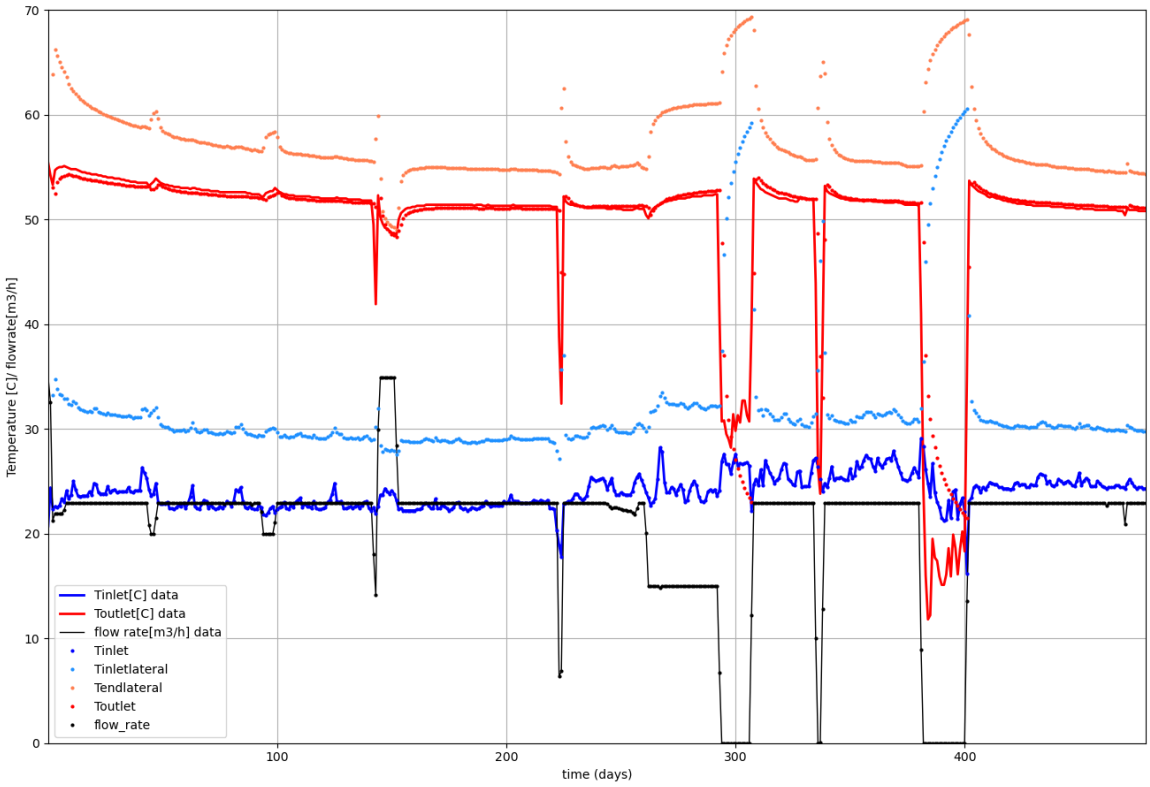

Figure 33 Thermal results of the Eavor Lite Loop simulations. Dots are the model simulations, (for more details on parameter settings see Van Wees et al., 2021).

Appendix B. Stress evaluation

The borehole stress evaluation is based on an analytical uni-axial stress solution for arbitrary oriented boreholes (Aadnoy and Chevenert, 1987; Aadnoy, 1988; Nguyen et al., 2009). The total stress response in the radial coordinates of the well:

$$\sigma_{rr} = \Delta P_w \frac{{r_w}^2}{r^2} + \left(\frac{\sigma_{xx}^0 + \sigma_{yy}^0}{2}\right)\left(1 - \frac{{r_w}^2}{r^2}\right) + \left(\frac{\sigma_{xx}^0 - \sigma_{yy}^0}{2}\right)\left(1 + 3\frac{{r_w}^4}{r^4} - 4\frac{{r_w}^2}{r^2}\right)\cos(2\theta)$$
$$+\sigma_{xy}^0\left(1 + 3\frac{{r_w}^4}{r^4} - 4\frac{{r_w}^2}{r^2}\right)\sin(2\theta)$$

$$\sigma_{\theta\theta} = -\Delta P_w \frac{{r_w}^2}{r^2} + \left(\frac{\sigma_{xx}^0 + \sigma_{yy}^0}{2}\right)\left(1 + \frac{{r_w}^2}{r^2}\right) - \left(\frac{\sigma_{xx}^0 - \sigma_{yy}^0}{2}\right)\left(1 + 3\frac{{r_w}^4}{r^4}\right)\cos(2\theta)$$
$$-\sigma_{xy}^0\left(1 + 3\frac{{r_w}^4}{r^4}\right)\sin(2\theta)$$

$$\sigma_{zz} = \sigma_{zz}^0 - 2\,\nu\left(\sigma_{xx}^0 - \sigma_{yy}^0\right)\frac{{r_w}^2}{r^2}\cos(2\theta) - 4\,\nu\,\sigma_{xy}^0\frac{{r_w}^2}{r^2}\sin(2\theta)$$

$$\sigma_{r\theta} = \left(0.5\left(\sigma_{xx}^0 - \sigma_{yy}^0\right)\sin(2\theta) - \sigma_{xy}^0\cos(2\theta)\right)\left(1 + 2\frac{{r_w}^2}{r^2} - 3\frac{{r_w}^4}{r^4}\right)$$

$$\sigma_{rz} = \left(\sigma_{xz}^0\cos(\theta) + \sigma_{yz}^0\sin(\theta)\right)\left(1 - \frac{{r_w}^2}{r^2}\right)$$

$$\sigma_{\theta z} = \left(-\sigma_{xz}^0\sin(\theta) + \sigma_{yz}^0\cos(\theta)\right)\left(1 + \frac{{r_w}^2}{r^2}\right)$$

Where ΔP_w is the change in well pressure relative to hydrostatic pressure and σ_{xx}^0, σ_{yy}^0, σ_{zz}^0 are the diagonal components of the in-situ effective stress tensor components in bore-hole coordinates, index z refers to the along hole axis, x, and y to cartesian coordinate-axes in the plane perpendicular to the along hole axis. θ is the azimuth in the x,y plane. σ_{xy}^0, σ_{xz}^0, σ_{yz}^0 are the off-diagonal components of the stress tensor.

Positive stress values are compressive.

The $\sigma_{rr}, \sigma_{\theta\theta}, \sigma_{zz}$ and $\sigma_{r\theta}, \sigma_{\theta z}, \sigma_{rz}$ correspond to the diagonal and off-diagonal components of the tensor of effective stress changes in radial coordinates, where θ represents azimuth and r the radius in the plane perpendicular to the borehole axis, corresponding to z-axis.

The thermal stress changes that are superposed to σ_{rr}, $\sigma_{\theta\theta}$ and σ_{zz} (cf. Tang and Luo, 1998) are:

$$\sigma_{rr}^T = \alpha\frac{E}{1-\nu}\frac{1}{r^2}\int_{r_w}^{r}(T(r') - T_0)\,r'dr'$$

$$\sigma_{\theta\theta}^T = \alpha\frac{E}{1-\nu}\left(T(r) - T_0 - \frac{1}{r^2}\int_{r_w}^{r}(T(r') - T_0)r'dr'\right)$$

$$\sigma_{zz}^T = \alpha\frac{E}{1-\nu}\left(T(r) - T_0\right)$$

Please note that the total stress complies to the boundary conditions that the change in radial stress at the borehole wall is equal to ΔP_w. The integral terms are evaluated through numerical integration of the thermal solution, assuming temperatures are constant in each grid cell.

The above implementation, excluding the effects of thermal stresses has been checked against the Kirsch stress solution (e.g. https://dnicolasespinoza.github.io/node44.html#SECTION00723000000000000000).

Appendix C. TNO Github

Git global setup

```
git config --global user.name "Jan Diederik van Wees"
git config --global user.email "jan_diederik.vanwees@tno.nl"
```

Create a new repository

```
git clone git@ci.tno.nl:AGS/Geothermal/eavor.git
cd eavor
git switch -c main
touch README.md
git add README.md
git commit -m "add README"
```

Push an existing folder

```
cd existing_folder
git init --initial-branch=main
git remote add origin git@ci.tno.nl:AGS/Geothermal/eavor.git
git add .
git commit -m "Initial commit"
```

Push an existing Git repository

```
cd existing_repo
git remote rename origin old-origin
git remote add origin git@ci.tno.nl:AGS/Geothermal/eavor.git
```